

Insights to the Binding of a Selective Adenosine A₃ Receptor Antagonist using Molecular Dynamics Simulations, Binding Free Energy Calculations and Mutagenesis

Panagiotis Lagarias,[†] Kerry Barkan,[‡] Eva Tzortzini,[†] Eleni Vrontaki,[†] Margarita Stampelou,[†] Graham Ladds,^{‡,*} Antonios Kolocouris^{†,*}

[†] Division of Pharmaceutical Chemistry, Department of Pharmacy, School of Health Sciences, National and Kapodistrian University of Athens, Panepistimioupolis-Zografou, 15771 Athens, Greece

[‡] Department of Pharmacology, University of Cambridge, Tennis Court Road, Cambridge, CB2 1PD, UK

Keywords: A₃ adenosine receptor, antagonist, mutagenesis, MM-PBSA, MM-GBSA, molecular dynamics

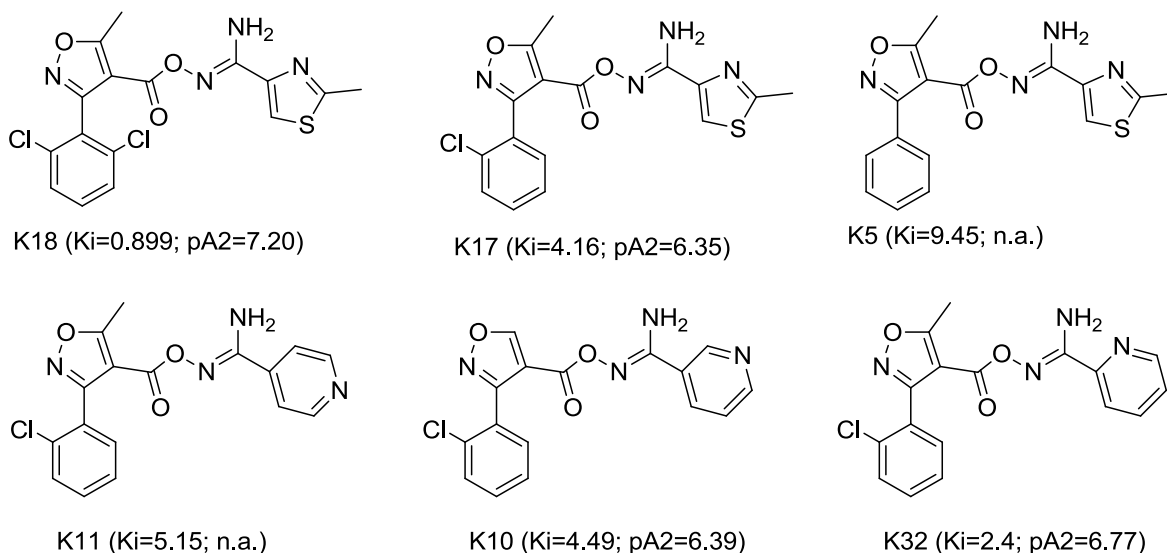
1 Abstract

Adenosine A₃ receptor (A₃R), is a promising drug target against cancer cell proliferation. Currently there is no experimentally determined structure of A₃R. Here, we have investigate a computational model, previously applied successfully for agonists binding to A₃R, using molecular dynamic (MD) simulations, Molecular Mechanics-Poisson Boltzmann Surface Area (MM-PBSA) and Molecular Mechanics-Generalized Born Surface Area (MM-GBSA) binding free energy calculations. Extensive computations were performed to explore the binding profile of O4-[[3-(2,6-dichlorophenyl)-5-methylisoxazol-4-yl]carbonyl]-2-methyl-1,3-thiazole-4-carbohydroximamide (K18) to A₃R. K18 is a new specific and competitive antagonist at the orthosteric binding site of A₃R, discovered using virtual screening and characterized pharmacologically in our previous studies. The most plausible binding conformation for the dichlorophenyl group of K18 inside the A₃R is oriented towards trans-membrane helices (TM) 5 and 6, according to the MM-PBSA and MM-GBSA binding free energy calculations, and by the previous results obtained by mutating residues of TM5, TM6 to alanine which reduce antagonist potency. The results from 14 site-directed mutagenesis experiments were interpreted using MD simulations and MM-GBSA calculations which show that the relative binding free energies of the mutant A₃R - K18 complexes compare to the WT A₃R are in agreement with the effect of the mutations, i.e. the reduction, maintenance or increase of antagonist potency. We show that when the residues V169^{5.30}, M177^{5.38}, I249^{6.54} involved in direct interactions with K18 are mutated to alanine, the mutant A₃R - K18 complexes reduce potency, increase the RMSD value of K18 inside the binding area and the MM-GBSA binding free energy compared to the WT A₃R complex. Our computational model shows that other mutant A₃R complexes with K18, including directly interacting residues, i.e. F168^{5.29}A, L246^{6.51}A, N250^{6.55}A complexes with K18 are not stable. In these complexes of A₃R mutated in directly interacting residues one or more of the interactions between K18 and these residues are lost. In agreement with the experiments, the computations show that, M174^{5.35} a residue which does not make direct interactions with K18 is critical for K18 binding. A striking results is that the mutation of residue V169^{5.30} to glutamic acid maintained antagonistic potency. This effect is in agreement with the binding free energy calculations and it is suggested that is due to K18 re-orientation but also to the plasticity of A₃R binding area. The mutation of direct interacting L90^{3.32} in the low region and the non-directly interacting L264^{7.35} to alanine in the middle region increases the antagonistic potency, suggesting that chemical modifications of K18 can be applied to augment antagonistic potency. The calculated binding energies ΔG_{eff} values of K18 against mutant A₃Rs displayed very good correlation with experimental potencies (pA₂ values). These results further approve the computational model for the description of K18 binding with critical residues of the orthosteric binding area which can have implications for the design of more effective antagonists based on the structure of K18.

2 Introduction

Adenosine is a naturally occurring purine nucleoside and an endogenous agonist of adenosine receptors.¹ The adenosine receptors are G protein-coupled receptors (GPCRs) comprising four subtypes; A₁, A_{2A}, A_{2B} and A₃. In particular, A_{2A} and A_{2B} subtypes act synergistically with the G_s proteins resulting in the stimulation of the adenylyl cyclase, and therefore, the increase of 3',5'-cyclic adenosine monophosphate (cAMP) levels. In contrast, A₁ and A₃ subtypes inhibit the adenylyl cyclase and decrease cAMP levels within a cell by coupling to G_i family of G proteins. Recent studies have shown that A₃R is over-expressed in various tumor cells.² This makes A₃R and its signaling pathway a promising drug target against cancer and for a number of other conditions like inflammatory diseases, including asthma and rheumatoid arthritis, glaucoma, chronic obstructive pulmonary disease and ischemic injury.¹ Experimentally resolved structures of A_{2A}R showing the binding mode of agonists, like adenosine and 5'-(N-ethylcarboxamido)adenosine (NECA),³⁻⁵ as well as of several antagonists i.e., CGS-21689,⁶ UK-432097,⁷ ZM241385,⁸⁻¹⁰ PSB36, caffeine and theophylline¹¹⁻¹⁴ and one bound to an engineered G protein⁴ have been determined since 2008.⁵ Experimental structures showed also the binding of A₁R with the antagonists DU172¹⁵ and PSB36^{16,17,18} and the adenosine-bound A₁R-G_i complex.¹⁹

These experimental A_{2A}R and A₁R structures provided excellent templates for structure-based drug design.^{20,21} In contrast, the experimental structure for A₃R has, to date, not been resolved. It has been observed that differences in the residues of the upper region of the orthosteric binding area define the selectivity of ligands against particular AR subtypes.²² The A₃R accommodates ligands having groups of increased lipophilicity fitted in the area close to V169^{5,30}. This lipophilic area in-between EL2, TM5 and TM6 is unique for A₃R and has a characteristic residue V169^{5,30}, while A₁R and A_{2A}R and A_{2B}R have a glutamic acid residue in the same position. As a first approach, we use a homology model of A₃R, built based on A_{2A}R in order to study the orthosteric binding area related to the function of this receptor. In our previous study, a fair description of the binding profile of the selective agonist IB-MECA and the non-selective NECA to A₃R was achieved through intensive computational work using the A₃R model, the application of MM-GBSA calculations and extensive mutagenesis.²³



Scheme 1. K18 and K11, K10, K32 which were measured experimentally in ref ²⁴. in parentheses are included the binding affinities from radiolabelled binding experiments and the antagonist potencies in micromolar concentrations; n.a. means an inactive compound in functional assays.

We have explored an *in silico* screening of 14,400 compounds of Maybridge HitFinder library against the X-ray structure of A_{2A}R complex bound with the selective antagonist ZM241385 using a combination of ligand- and structure-based approaches. ²⁵ Of particular interest for further development was the class of carboximidamide derivatives of which K18 was identified as a potent and selective A₃R antagonist in a previous study (Scheme 1). ²⁴ In that research, ²⁴ we studied experimentally the effect of mutations L90^{3,32}, V169^{5,30}, M174^{5,35}, M177^{5,38}, I249^{6,54}, I253^{6,58}, L264^{7,35}, W185^{5,46}/V169^{5,30} to alanine within the orthosteric binding area of A₃R to the antagonistic potency of K18. ²⁴ The I253^{6,58}E, V169^{5,30}E mutants were also explored. Furthermore, in another study we performed mutagenesis and intensive computational work to investigate the binding profile of the selective agonist 1-deoxy-1-[6-[(3-iodophenyl)methyl]amino]-9H-purin-9-yl]-N-methyl-β-D-ribofuranuronamide (IB-MECA) and the non-selective NECA to A₃R. ²³ A fair description was accomplished using homology models for the mutant A₃R_s and the amber99sb force field and through the application of MM-GBSA binding free energy calculations.

As a continuation of these studies, we aimed to investigate, in detail, the binding profile and binding area of the antagonist K18. K17 was also found to be competitive antagonist in the previous study, although less potent compared to K18, having less one chloride atom connected with the phenyl group. Commercial compound libraries have not available dichlorophenyl analogues of K18, and seeking to study the effect of modifying additional fragments of the active chemical probe, we purchased compounds K11, K10 and K32 analogues of K17 (Scheme 1). K11, K10 and K32 have a pyridinyl substituent, instead of 1,3-thiazolyl, which is linked with carbonyloxycarboximidamide linker through

C2, C3 and C4 carbons, respectively. K32, K10 show potent antagonistic potency while K11 is inactive. We applied MD simulations and MM-PBSA, MM-GBSA calculations^{26,27} in the complexes of K18, K32, K10, K11 with WT A₃R to study the interactions of the ligands with orthosteric binding area and the residues involved in binding with higher interaction frequency. The stability of complexes between K18 and 14 A₃R mutated receptors is investigated computationally through MD simulations and MM-GBSA calculations and compare with the experimental site-directed mutagenesis results.²¹

2 Methods

Computational Biochemistry

Preparation of Receptor Structures - Molecular docking calculations

Receptor structures. The complex of the inactive form of the WT A_{2A}R (PDB ID 3EML)¹¹ with ZM241385 was superimposed to the model of inactive WT A₃R (N12^{1,32} - H304^{7,75}) derived from Adenosiland web-service²⁸ that was built using the crystal structure of PDB ID 3EML as template²⁸ (numbers in parentheses refer to the Ballesteros–Weinstein numbering²⁹). The inactive protein conformation of A_{2A}R was removed resulting in the ZM241385-inactive WT A₃R model. In the A₃R WT model, the side chain of V169^{5,30} was rotated as suggested³⁰ to increase the free space for the accommodation of agonists with bulky substitutions.³¹ The ZM241385-inactive A_{2A}R protein complex (PDB ID 3EML)¹¹ was superimposed to NECA-active A_{2A}R protein complex with PDB ID 2YDV.³ Then the NECA and inactive protein conformation were removed resulting in ZM241385-active A_{2A}R complex model. As a next step, the ARs were optimized using the Protein Preparation Wizard implementation in Schrodinger suite.³² In this process, the bond orders and disulfide bonds were assigned, and missing hydrogen atoms were added. Additionally, N- and C-termini of the protein model were capped by acetyl and N-methyl-amino groups, respectively. The systems were subjected in an all-atom minimization using the OPLS2005 force field³³ with heavy atom RMSD values constrained to 0.30 Å.

After MD simulation of the K18-A₃R complex, the equilibrated structure was used for the preparation of the mutant receptor models of WT A₃R complex by changing the studied residues to alanine, through the "Build" tool of Maestro. The 14 mutant A₃R mentioned in the last paragraph of the introduction section in complex with K18 were subjected in minimization using the previously used protocol.

Docking calculations. K18 was prepared for docking calculations using Maestro.³⁴ The ZM241385-inactive WT A₃R model was used as a template for docking of K18 in the *apo* A₃R. For this purpose, ZM241385, utilized as a reference ligand, and *apo* protein WT A₃R were saved separately. Ligand binding site was defined within 10 Å of ZM241385 coordinates. Molecular docking calculations of the energy minimized form of K18 were performed using GoldScore³⁵ scoring function in GOLD 5.2 software,³⁵⁻³⁷ applying 30 genetic algorithm runs. The “allow early termination” option, which terminates ligand searching if the top three solutions have an RMSD difference less than 1.5 Å was inactivated, and the “Generate Diverse Solutions” option, which sets smallest inter-cluster RMSD to 1.5 Å, was activated. All other parameters were set to their default values. The resulting highest-scoring pose had the dichlorophenyl group with an orientation towards TM5, TM6 and the second one had the dichlorophenyl group with an orientation towards TM1, TM2. From now on we will refer to these conformations as "up TM5, TM6" and "up TM1, TM2". For the investigation of the most likely conformation of K18 inside the WT A₃R we kept the 6th scored docking pose with the isoxazole-dichlorophenyl instead of the thiazole ring oriented deep in the A₃R. This will be referred as "down" conformation

A set of 75 structures were selected from PubMed based on their best similarity with K18 using TanimotoCombo metric, which is the sum of the ShapeTanimoto (metric of shape) and ColorTanimoto (metric of functional group) scores,³⁸ and were prepared for docking calculations using Maestro.³⁴ The energy minimized form of these 75 structures was docked in the inactive form of WT A₃R using Glide XP; the docking poses produced were subjected to Induced Fit Docking (IFD).³⁹ The commercially available compounds K40-K43 which contain both 3-(dichlorophenyl)-5-methylisoxazole and thiazole were selected, purchased and biologically tested.

The 14 mutant A₃R_s in complex with the best docking pose of K18 in the WT A₃R were used for molecular docking calculations using the same procedure described above.

MD simulations between ligands and A₃R

MD simulations of K18, K40-K44 with WT A₃R. Complexes of the previously mentioned K18 conformations i.e., "up TM5, TM6", "up TM1, TM2" and "down", molecules K40-K44 with the WT A₃R model were inserted in a pre-equilibrated hydrated POPE membrane bilayer. The MD simulations were performed with Desmond software and the OPLS2005. The orthorhombic periodic box boundaries were set 15 Å away from the protein atoms. The system contained 150 lipids, 15,000 water molecules corresponding to the TIP3P water model and salt concentration 0.15M NaCl and was built using the System Builder utility of Desmond.^{40,41,42} The total number of atoms of each complex was approximately ~70,000. Desmond Viparr tool was used to assign amber99sb force field parameters^{43,44} to protein and

lipid, and GAFF⁴⁵ was used for the parameters of the ligand. Initial ligand parameters were constructed with the antechamber module of Amber14.⁴⁶ MD simulations were performed at 310 K in order to ensure that the membrane state is above the main phase transition temperature of 298 K for POPE bilayers.⁴⁷

The MD simulations were also performed at 310 K using a buffered orthorhombic system in 10 Å distance from the solute atoms with periodic boundary conditions for all the complexes using AMBER14 software. Each complex-bilayer system was processed by the LEaP module in AmberTools14 under the AMBER14 software package.⁴⁸ Amberff14SB force field parameters⁴⁹ were applied to the protein, lipid14 to the lipids,⁵⁰ Generalized Amber Force Field (GAFF) to the ligands⁴⁵ and TIP3P⁵¹ to the water molecules for the calculation of bonded, van der Waals and electrostatic interactions. Atomic charges were computed according to the RESP procedure⁵² using Gaussian03⁵³ and antechamber module of AmberTools14.⁴⁸ The MD simulations protocols are described in the Supporting Information.

In the production phase, the relaxed systems were simulated in the NPT ensemble conditions for 100 ns. Within this simulation time, the total energy and the RMSD of the protein's backbone C α atoms reached a plateau, therefore the systems were considered equilibrated and suitable for statistical analysis.

MD simulations of K18 with mutant A₃Rs. The stability of the complexes between K18 and the 14 mutant A₃Rs was investigated using MD simulations for 100 ns with Schrodinger Desmond Maestro v11.1 and the amber99sb force field using the same protocol described above. Within this simulation time, the total energy and RMSD of the of the protein backbone C α atoms reached a plateau, and the systems were considered equilibrated and suitable for statistical analysis.

Analysis of MD simulations trajectories. The visualization of produced trajectories was performed using the GUI of Maestro and the protein-ligand interaction analysis was done with the Simulation Interaction Diagram (SID) tool, available with Schrodinger Desmond Maestro v. 11.1. For hydrogen bond interactions, a distance of 2.5 Å between donor and acceptor heavy atoms, and an angle $\geq 120^\circ$ between donor-hydrogen-acceptor atoms and $\geq 90^\circ$ between hydrogen-acceptor-bonded atom were considered. Non-specific hydrophobic contacts were identified when the side chain of a hydrophobic residue fell within 3.6 Å from a ligand's aromatic or aliphatic carbon, while π - π interactions were characterized by stacking of two aromatic groups face-to-face or face-to-edge. Water-mediated interactions were characterized by a distance of 2.7 Å between donor and acceptor atoms, as well as an angle $\geq 110^\circ$ between donor-hydrogen-acceptor atoms and $\geq 80^\circ$ between hydrogen-acceptor-bonded atom. The visualization of produced trajectories and structures was performed using the programs Chimera⁵⁴ and VMD.⁵⁵ All the MD simulations were run on GTX 1060 GPUs in lab workstations or on the ARIS Supercomputer.

MM-PBSA and MM-GBSA calculations

The effective binding free energies (ΔG_{eff}) of the complexes between the three docking poses of K18, K40-K43 and A₃R complexes were computed considering the gas phase energy and solvation free energy contributions to binding⁵⁶ using the 1-trajectory MM-PBSA, MM-GBSA approach.⁵⁷ For this, structural ensembles for each complex were extracted every 50 ps from the last 50 ns of the production simulations. Prior to the calculations all water molecules, ions, and lipids were removed, and the structures were positioned such that the geometric center of each complex was located at the coordinate origin. For MM-PBSA calculations, molecular mechanics energies and the non-polar contribution to the solvation free energy were computed with the *mmpbsa.pl* module⁵⁸ of Amber14.⁴⁸ For MM-GBSA calculations the relevant module in Schrodinger Suite was used, i.e. the *thermal_mmgbsa.pyscript* that takes individual trajectory snapshots and calculates ΔG_{eff} and its energetic contributions (see Supporting Information).

3 Results and Discussion

Validation of the force field for the MD simulations

Since there is no experimental structure for A₃R, we chose A_{2A}R to test a computational model that can be accurate for our calculations with antagonists. In a previous paper we tested how different force fields describe the interactions between agonist NECA and the orthosteric binding area of A_{2A}R in the experimental structure. We found that amber99sb can accurately describe the interactions as well as the conformation of helical TM regions.²³ Here, we test the performance of amber99sb force field for an antagonist-A_{2A} complex using the experimental structures of A_{2A}R in the active³ and the inactive state.^{59,10} We tested if amber99sb can produce conformational changes that ZM241385 binding can effect to the active state of A_{2A}R towards the complex of ZM241385 with the inactive state of A_{2A}R.^{59,10} Thus, 500 ns MD simulation of ZM213485 in complex with the active conformation of A_{2A}R (PDB ID 2YDV)³ in hydrated POPE bilayers was performed using the amber99sb force field to test if this force field can describe the conformational change leading to an intermediate conformation of the inactive state of A_{2A}R.

59,10

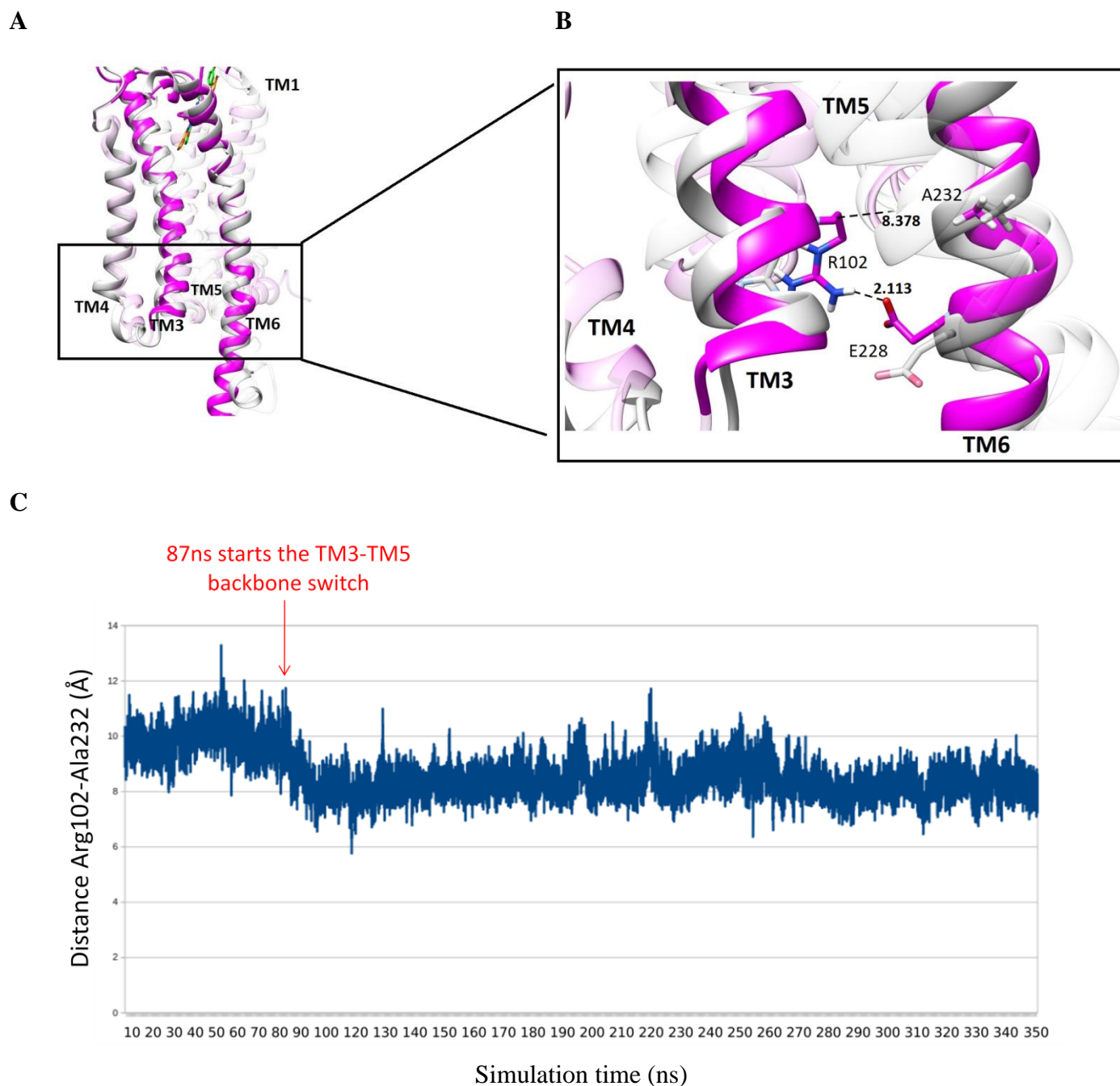


Figure 1. (A), (B) The decrease in the distance between TM3-TM6 caused the formation of the ionic lock between R102^{3.50} and E228^{6.30}. (C) Separation between TM3-TM5 for the 350 ns MD simulation; the distance between R102^{3.50} and A232^{5.34} C α carbons decreased from ca 11 to 7.5 Å.

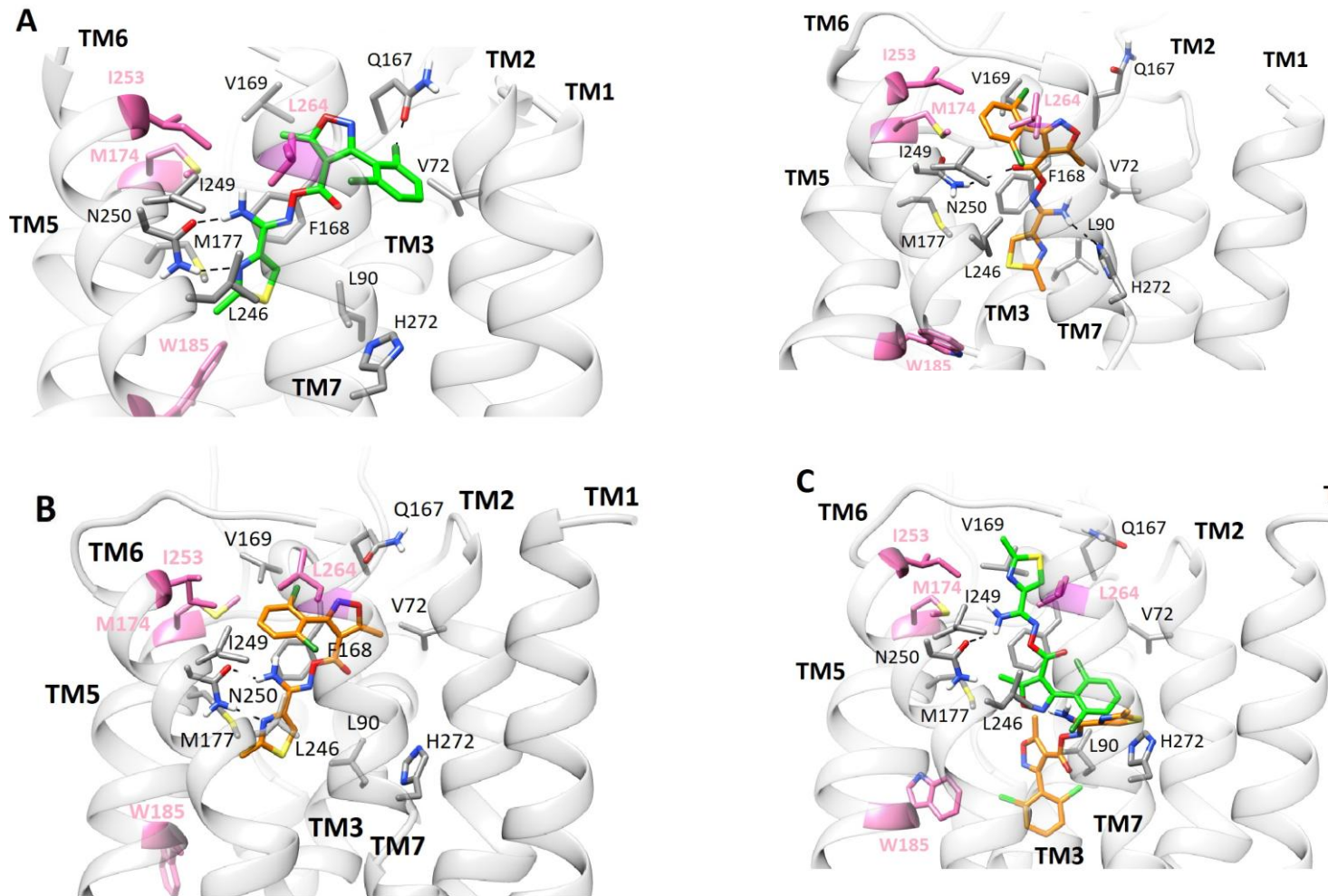
After 300 ns of simulation the ZM241385-active A_{2A}R complex adopted an inactive-like conformation of A_{2A}R having an RMSD of ca 2 Å compared to the experimental structure PDB ID 3EML.¹¹ The conformational changes observed are: (a) decrease in the distance between TM3-TM6; the distance between R102^{3.50} and A232^{6.34} C α carbons changed from 11 to 7.5 Å (Figure 1,C). (b) decrease in the distance between TM3-TM5; the distance between I104^{3.52} and I200^{5.61} C α carbons decreased from 11 to 9.8 Å. (c) significant change in χ_1 , χ_2 dihedrals values of residue W243^{6.48} from -80°, -120° to -70°, +90° respectively; this change in the dihedrals caused W243^{6.48} indole ring placement almost horizontal to TM3. (d) formation of the ionic lock between R102^{3.50} and E228^{6.30}. These measures showed that

amber99sb force field is sensitive in describing A_{2A}R receptor conformational changes and can be applied for the simulations of antagonists like K18 in complex with A₃R. In addition, our previous study suggested that amber99sb is suitable for the simulations of agonist nucleosides in complex with adenosine receptors.²³

MD simulations of K18 and congeneric compounds in complex with WT A₃R

The MD simulation with the "up TM5, TM6" conformation (see methods section) as starting structure converged in a stable conformation with an RMSD of less than 2 Å compared to the starting structure.²⁴ Interestingly, the MD simulations revealed that starting from conformation "up TM1, TM2", K18 rotated phenyl-oxazolyl bond but also N-O bond resulting in a conformation with a dichlorophenyl orientation also towards TM5, TM6 conformation (Figure 2A) with a relative binding free energy $\Delta\Delta G_{\text{eff}} = + 3.8$ compared to "up TM5, TM6" starting structure conformation (Figure 2B) according to both MM-PBSA and MM-GBSA calculations.

The MD simulations of K18 in complex with WT human A₃R showed that the most frequent (>20% of the MD trajectory) contacts involved V72^{2,23}, L90^{3,32}, F168^{5,29}, V169^{5,30}, M177^{5,38}, L246^{6,51}, I249^{6,54}, N250^{6,55} as previously found,²⁴ and less than 15% was recorded for van der Waals with V65^{2,16}, I186^{5,47} and L264^{7,35}. Hydrophobic contacts were measured in the MD simulations and are showed in the interaction fraction plot (Figure 2D) when the side chain of a hydrophobic residue fell within 3.6 Å from the ligand. In particular, as shown in the binding conformation the phenyl group of the 3-phenyl-isoxazole interacts through attractive van der Waals forces with V169^{5,30} and I249^{6,54} and the isoxazole adopts an aromatic π - π stacking interaction with the phenyl group of F168^{5,29}. Nitrogen and oxygen atoms of isoxazole can be hydrogen bonded to NH groups of F168^{5,29} or V169^{5,30}. The thiazolyl group can be hydrogen bonded to N250^{6,55} and have van der Waals interactions with L90^{3,32}, M177^{5,38}, L246^{6,51} and V72^{2,23}. The "down" conformation of K18 was unstable, the ligand lost binding interactions and shifted away the binding area (Figure 2C). MM-PBSA calculations^{57,56} further supported the "up TM5, TM6" conformation of K18 since, as described in ref. 24 the relative ΔG_{eff} values between K18 and two congeners having one or no chlorine atoms, i.e. compounds K17 and K5 (Scheme 1), were in agreement with experimental binding affinities and activities.²⁴ K17 having one chlorine atom in the phenyl ring compared to K18 had antagonistic potency and similar binding profile to K18 (Scheme 1, Figure S1).²⁴ In contrast K5 with no chlorine atoms lack of antagonistic potency. In contrast the "up TM1, TM2" conformation did not account for the relative experimental binding free energy differences.



D

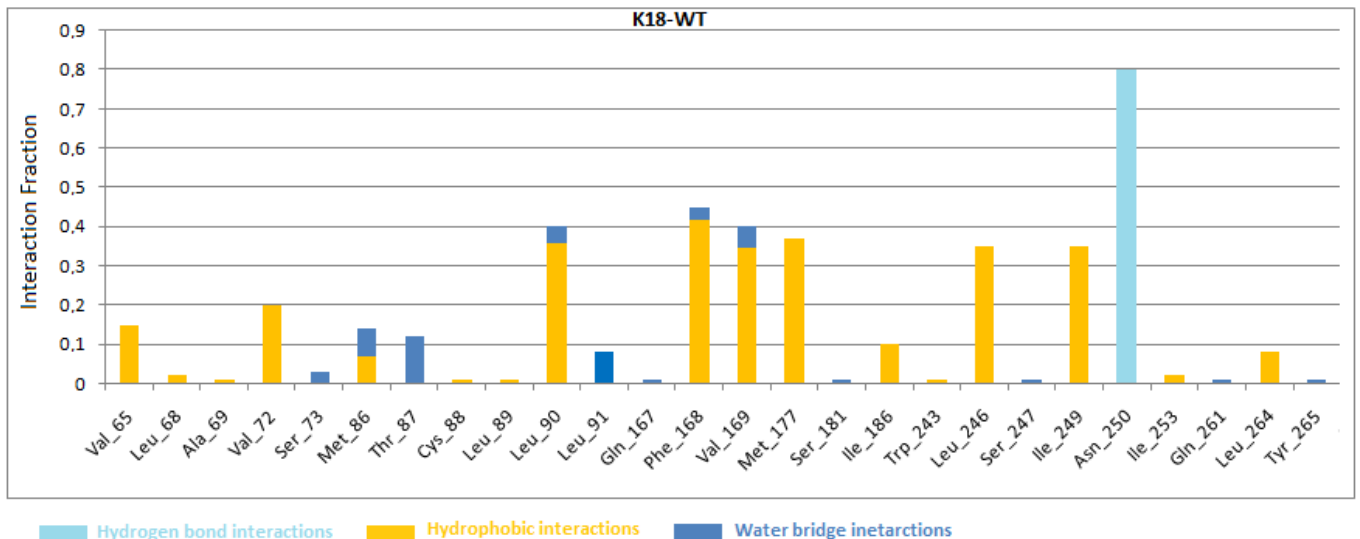


Figure 2. (A) (left) Starting structure of K18 in the "up TM1, TM2" conformation (carbon atoms in green) inside WT A₃R and (right) average structure from 100 MD simulations (carbon atoms in yellow). (B) Average structure of K18 from 100 MD simulations in the "up TM5, TM6" conformation (carbon atoms in yellow), and (C) Starting structure of K18 in the "down" conformation (carbon atoms in green) inside WT A₃R and average structure from 100 MD simulations (carbon atoms in yellow). The side

chains of residues involved in ligand binding, separated by 3.6 Å from the ligand and having interaction frequencies ≥ 0.2 are displayed as gray sticks. Protein structure is displayed in grey ribbons. In pink residues which were mutated to alanine but are more than 4 Å apart from the ligand are displayed. Hydrogen atoms are omitted except for those involved in hydrogen bond interactions which are highlighted as black dashed lines. (D) Receptor-ligand interaction histogram interactions plot of K18 "up TM5, TM6" conformation inside A₃R for 150 ns of MD simulations. Hydrogen bonding interactions bar is depicted in light blue, van der Waals in yellow, water bridges in blue. Bars are plotted for residues with interaction frequencies ≥ 0.2 .

A congeneric series to K17 are compounds K11, K10 and K32 having a pyridinyl substituent, instead of 1,3-thiazolyl, which is linked with carbonyloxycarboximidamide linker through C2, C3 and C4 carbons, respectively. K11, K10 and K32 have more similar structure to K17 compared to K18, having one chlorine atom in the phenyl ring rather than two chlorine atoms in K18. Since, we found no commercially available the pyridine analogues to K18 we have explored K17 derivatives aiming at improving potency of K18 by investigating structure-activity relationships of various parts of the molecule.

The MD simulations suggested that compound K32 can form an additional hydrogen bond interaction with N250^{6,55} through 2-pyridinyl nitrogen (Figure 3C) and also has a 2-fold higher affinity than K10, K11. K10 also formed a hydrogen bond between pyridinyl nitrogen with S247^{6,52} (Figure 3B). The binding free energy values derived from MM-PBSA calculations (ΔG_{eff}) fairly agree with this ranking (Table 1) supporting the proposed binding mode of K18. However, the biological assays showed that K32 and K10 are competitive antagonists like K17, but K11 did not have any effect on signaling below the tested concentration of 10 μM , suggested that antagonistic potency cannot be correlated directly with affinity.

Table 1. Effective binding energies (ΔG_{eff}) and energy components (E_{vdw} , E_{EL} , ΔG_{solv}) in kcal mol⁻¹ calculated using the MM-PBSA method for K10, K11 and K32 binding to the A₃R orthosteric site.

	E_{vdw}^1	E_{EL}^2	ΔG_{solv}^3	ΔG_{eff}^4	Schild analysis ⁵	Radioligand binding ⁶
	Conformation "up TM5, TM6"					
K10	-39.7 ± 0.2	-9.0 ± 0.2	23.7 ± 0.2	-25.0 ± 0.2	6.39 ± 0.3	4.49
K11	-38.7 ± 0.2	-9.7 ± 0.1	23.9 ± 0.2	-24.4 ± 0.2	n.a.	5.15
K32	-39.3 ± 0.2	-6.6 ± 0.2	20.0 ± 0.2	-25.8 ± 0.2	6.77 ± 0.3	2.40

¹ Van der Waals energy of binding calculated using molecular mechanics

² Electrostatic energy of binding calculated using molecular mechanics

³ Difference in solvation energy between the complex, the protein and the ligand, i.e. $G_{\text{complex, solv}} - (G_{\text{protein, solv}} + G_{\text{ligand, solv}})$

⁴ Effective binding free energy calculated as $\Delta G_{\text{eff}} = \Delta E_{\text{MM}} + \Delta G_{\text{solv}}$; in Table 1, $\Delta E_{\text{MM}} = E_{\text{vdw}} + E_{\text{EL}}$ (see Materials and Methods Section)

⁵ pK_B obtained through Schild analysis in A₃R stably expressing Flp-In CHO cells.²⁴

⁶ K_i values (μM) previously published for K5, K17 and K18⁶⁰ through radio-ligand binding assays.

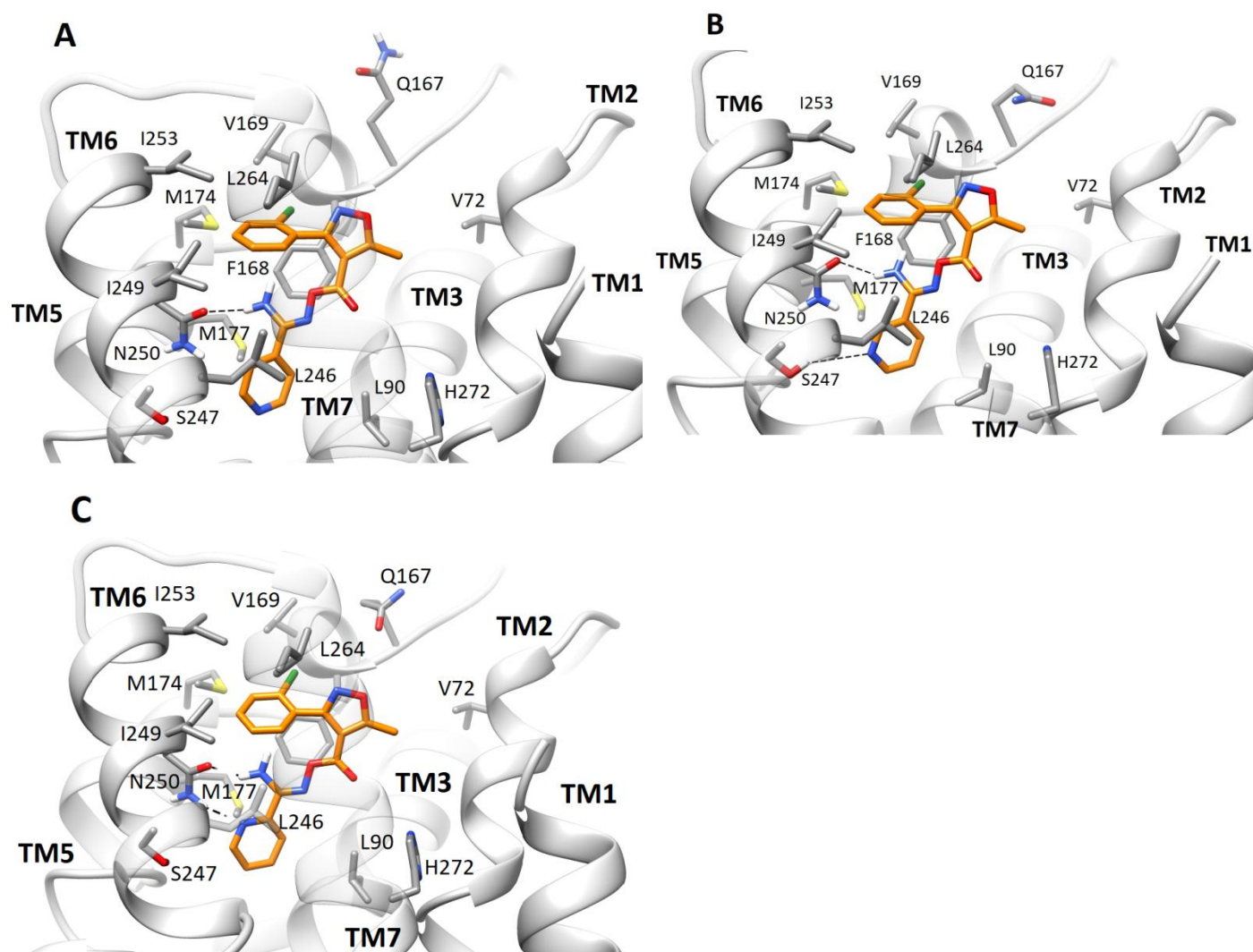


Figure 3. (A)-(C) Average structure of K11, K10 and K32 in the "up TM1, TM2" conformation inside WT A₃R from 100 MD simulations (carbon atoms in yellow).

Searching in commercial libraries by applying similarity-based parameters (TanimotoCombo³⁸ coefficient > 0.65) with K18, we found only compounds K40-K43 (Scheme S1) which include, like K17, the chlorophenyl-5-methylisoxazole and the 2-methyl-1,3-thiazole, but connected through a different linker from the carbonyloxycarboximidamide linker in K17, K18. All compounds were inactive and the MD simulations show their unstable binding. (see SI for the relevant discussion and Figure S2).

Simulations of K18 in complex with mutant versions of A₃R

MM-GBSA binding free energy calculations. In order to investigate computationally the stability and the interactions for each mutant A₃R-agonist complex with K18 their complexes in a hydrated POPE bilayer were subjected to MD simulations for 150 ns and MM-GBSA calculations were performed in the resulting trajectories. The previously experimentally determined pA₂ values²⁴ were included in Table 2; it is recalled that an increase in the pA₂ value of K18 for a particular mutant A₃R (when compared to WT A₃R) shows that the antagonist was more active and a decrease indicated a reduced potency. The pA₂ values and the calculated effective binding free energies (ΔG_{eff})^{57,56} (Table S1, Figure S3) showed significant correlation for K18 $r = -0.82$ (95% confidence interval, -0.94 to -0.68 (n=12), $p < 0.01$) (Figure 4). In a previous study, the binding free energy calculations of agonists in complex with A₃Rs using the MM-GBSA method showed also fair correlation.²³

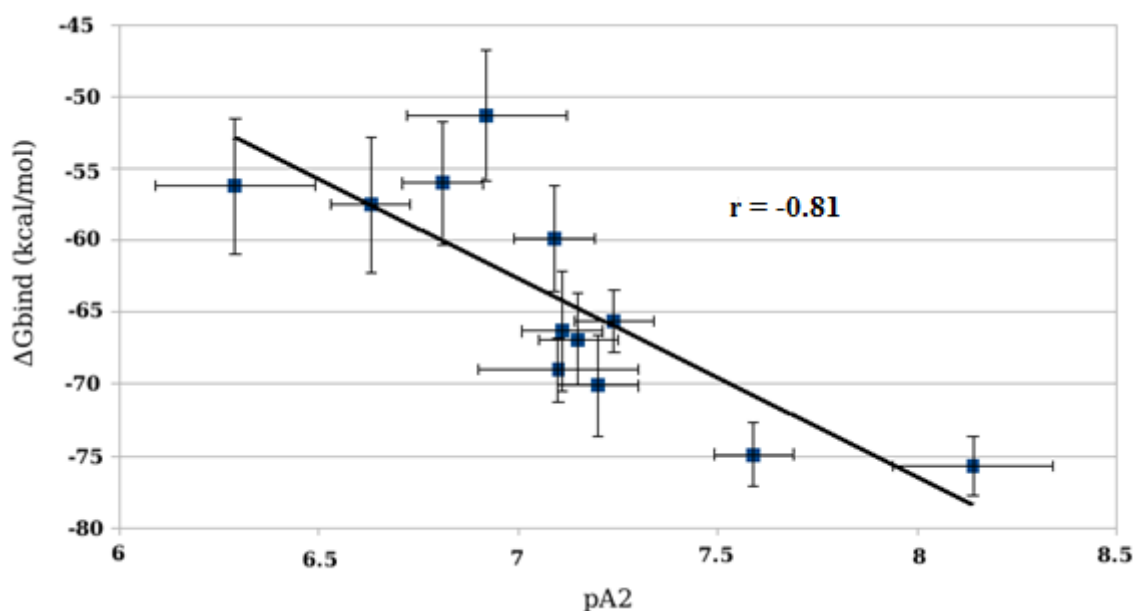


Figure 4. Binding free energies of K18 computed by the MM-GBSA method (ΔG_{eff}) plotted against experimental activities (pIC₅₀) for several mutant A₃Rs. Maximal errors in assays pA₂ and ΔG_{eff} are shown as error bars along the vertical and horizontal axes, respectively.

We observed that mutants V169^{5.30}A, M174^{5.35}A, M177^{5.38}A, W185^{5.46}A/V169^{5.30}A, which led to reduction or loss of potency of K18, display relative binding free energy values ($\Delta\Delta G_{\text{eff}} = \Delta G_{\text{eff,mut}} - \Delta G_{\text{eff,WT}}$) for the studied agonist greater than +10 kcal mol⁻¹ compared to the WT receptor (Table 2, Figure S3). Similarly, the calculations also show that the complexes of K18 with mutant F168^{5.29}A, L246^{6.51}A, N250^{6.55}A A₃Rs are not favored (Table 2). The effect of mutant F168^{5.29}A, L246^{6.51}A and N250^{6.55}A A₃Rs can not be explored experimentally by mutagenesis. These receptors produce no detecting response to K18 since the agonist was not active. Mutant receptors V169^{5.30}E, W185^{5.46}A,

I249^{6.54}A, I253^{6.58}A, I253^{6.58}E that maintain or increase activity of the studied have relative binding free energies $\Delta\Delta G_{\text{eff}}$ that were 1-4.5 kcal mol⁻¹ more positive than K18-WT A₃R except I249^{6.54}A with a $\Delta\Delta G_{\text{eff}}$ of ca 10 kcal mol⁻¹ (Table 2, Figure S3). Mutants L90^{3.32}, L264^{7.35}A that increase the potency of the studied antagonist agonist have relative binding free energies $\Delta\Delta G_{\text{eff}}$ that were -5.6 and -4.8 kcal mol⁻¹ more negative than K18-WT A₃R. While more accurate computational methods like FEP/MD⁶¹ are available the calculated $\Delta\Delta G_{\text{eff}}$ values using the MM-GBSA allowed us to distinguish the reduction, maintenance and increase of K18 potency against the corresponding mutant A₃R receptors.

Table 2. Antagonistic potencies and MM-GBSA calculated relative binding free energies ($\Delta\Delta G_{\text{eff}}$ in kcal mol⁻¹) of K18 in complex with WT and mutant A₃Rs.

Mutant A ₃ R	A ₃ R region	$\Delta\Delta G_{\text{eff}}$ ^a	pA ₂ ^b	RMSD _{protein} ^c	RMSD _{lig} ^d	Potency
WT	-	0	7.20 ± 0.1 ^f	2.00 ± 0.1	1.67 ± 0.26	baseline
L90 ^{3.32} A	Low	-5.6 ± 0.01	8.14 ± 0.2	2.43 ± 0.1	3.67 ± 0.44	increase
F168 ^{5.29} A	Middle	+15.1 ± 0.03	N.R. ^e	3.30 ± 0.2	6.02 ± 0.32	N.R. ^e
V169 ^{5.30} A	Middle	+14.1 ± 0.1	6.81 ± 0.1	2.25 ± 0.1	4.53 ± 0.27	decrease
V169 ^{5.30} E	Middle	+3.2 ± 0.03	7.15 ± 0.1	2.70 ± 0.2	3.54 ± 0.31	baseline
M174 ^{5.35} A	Middle	+12.6 ± 0.1	6.63 ± 0.2	2.48 ± 0.1	5.14 ± 0.67	decrease
M177 ^{5.38} A	Middle	+13.9 ± 0.1	6.29 ± 0.2	3.07 ± 0.1	6.66 ± 0.31	decrease
W185 ^{5.46} A	Low	+1.1 ± 0.1	7.10 ± 0.1	2.55 ± 0.1	6.82 ± 0.41	baseline
V169 ^{5.30} A/W185 ^{5.46} A	Middle/Low	+18.8 ± 0.1	6.92 ± 0.1	2.17 ± 0.1	5.30 ± 0.26	decrease
L246 ^{6.51} A	Middle	+15.7 ± 0.1	N.R. ^e	2.38 ± 0.1	6.38 ± 0.69	N.R. ^e
I249 ^{6.54} A	Middle	+10.2 ± 0.01	7.09 ± 0.1	2.47 ± 0.2	2.87 ± 0.35	baseline
N250 ^{6.55} A	Middle	+1.1 ± 0.1	N.R. ^e	2.21 ± 0.2	5.95 ± 0.58	N.R. ^e
I253 ^{6.58} A	Middle	+4.5 ± 0.1	7.24 ± 0.1	3.52 ± 0.2	3.56 ± 0.32	baseline
I253 ^{6.58} E	Middle	+3.8 ± 0.05	7.11 ± 0.1	2.48 ± 0.1	3.63 ± 0.21	baseline
L264 ^{7.35} A	Middle	-4.8 ± 0.1	7.59 ± 0.1	2.44 ± 0.3	3.50 ± 0.20	increase

^a Relative binding free energy (kcal mol⁻¹) between mutant and WT receptors ($\Delta G_{\text{eff,mutant}} - \Delta G_{\text{eff,WT}}$). ΔG_{eff} is calculated from the last 50 ns of the trajectories using 50 ps intervals (i.e. 1000 frames per trajectory). See also Table S1.

^b Antagonists potency as determined via Schild analysis.²⁴

^c Mean ± SD (Å); Protein RMSD is calculated for the C_α atoms of the α-helices, for the last 50 ns of the trajectories. Frame 0 is used as reference structure.

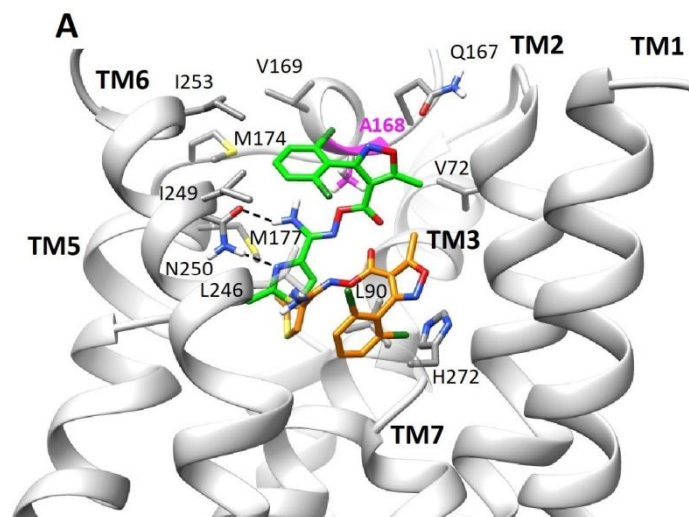
^d Mean ± SD (Å); Ligand RMSD is calculated after superposition of each protein-ligand complex to that of frame 0 (reference structure) based on the C_α atoms of the protein, for the last 50ns of the trajectories.

^e N.R.; no response, denotes no agonist activity preventing determination of K18 activity using Schild analysis

^f Mean absolute error.

Receptor mutations that led to loss or reduction of antagonistic potency. Mutations of residues that are positioned in EL2, TM5, TM6 i.e. V169^{5.30}, M174^{5.35}, M177^{5.38}, W185^{5.46}/V169^{5.30} to alanine reduce antagonistic potency compared to the WT A₃R. This result further supported the suggested "up TM5-TM6" conformation for K18 since the loss of the attractive van der Waals interactions with residues in TM5 and TM6, i.e. V169^{5.30}, M177^{5.38}, I249^{6.54} led to the decrease of antagonistic potency. As mentioned before, mutant F168^{5.29}A, L246^{6.51}A and N250^{6.55}A A₃R_s produced no detecting response since the agonist was not active. Except from M174^{5.35}, all the other residues are in contact with the ligand according to Figure 2.

From the corresponding trajectories for the F168^{5.29}A, L246^{6.51}A, N250^{6.55}A, M174^{5.35}A, M177^{5.38}A A₃R_s, it was clear that K18 was unstable inside the receptor area probably because of the significant displacement of the ligand from its starting binding conformation during the MD simulations as suggested by the high RMSD_{lig} values of ca 4.5-7 Å and $\Delta\Delta G_{\text{eff}}$ of +13 to +16 kcal mol⁻¹ (Table 2, Figures S3-S5). For example, the π - π interactions between F168^{5.29} and the oxazole ring of the ligand are absent in the mutant F168^{5.29}A and this results in the decrease of the hydrogen bond interactions with the critical N250^{6.55} and van der Waals interactions with V169^{5.30} (Figure 5). The ligand translocates from its starting binding conformations, drifts deeper in the receptor and waters enter the binding area, resulting in an unstable binding mode which is consistent with the $\Delta\Delta G_{\text{eff}}$ of +15 kcal mol⁻¹ compared to the WT A₃R. In the V169^{5.30}A-K18 or M177^{5.38}A or L246^{6.51}A complexes the ligand has an RMSD_{lig} of ca 4.5 Å and a $\Delta\Delta G_{\text{eff}}$ of ca +14 kcal mol⁻¹ or ca 6.7 Å and a $\Delta\Delta G_{\text{eff}}$ of ca +14 kcal mol⁻¹ or ca 6.4 Å and a $\Delta\Delta G_{\text{eff}}$ of ca +16 kcal mol⁻¹ (SI, Figure S4, S6, S7). The functional assays suggest that M174^{5.35} is also an important residue, since its mutation to alanine led to a reduction of antagonistic potency which is consistent with the RMSD_{lig} of ca 5 Å and a $\Delta\Delta G_{\text{eff}}$ of +13 kcal mol⁻¹ (Figure S5). According to the interactions plot from our computational study this residue did not make direct interactions with the WT A₃R. Although M174^{5.35} is ca 4 Å far from K18, it is positioned between I253^{6.58} and V169^{5.30} and contributes significantly to the stabilization of the binding area.



B

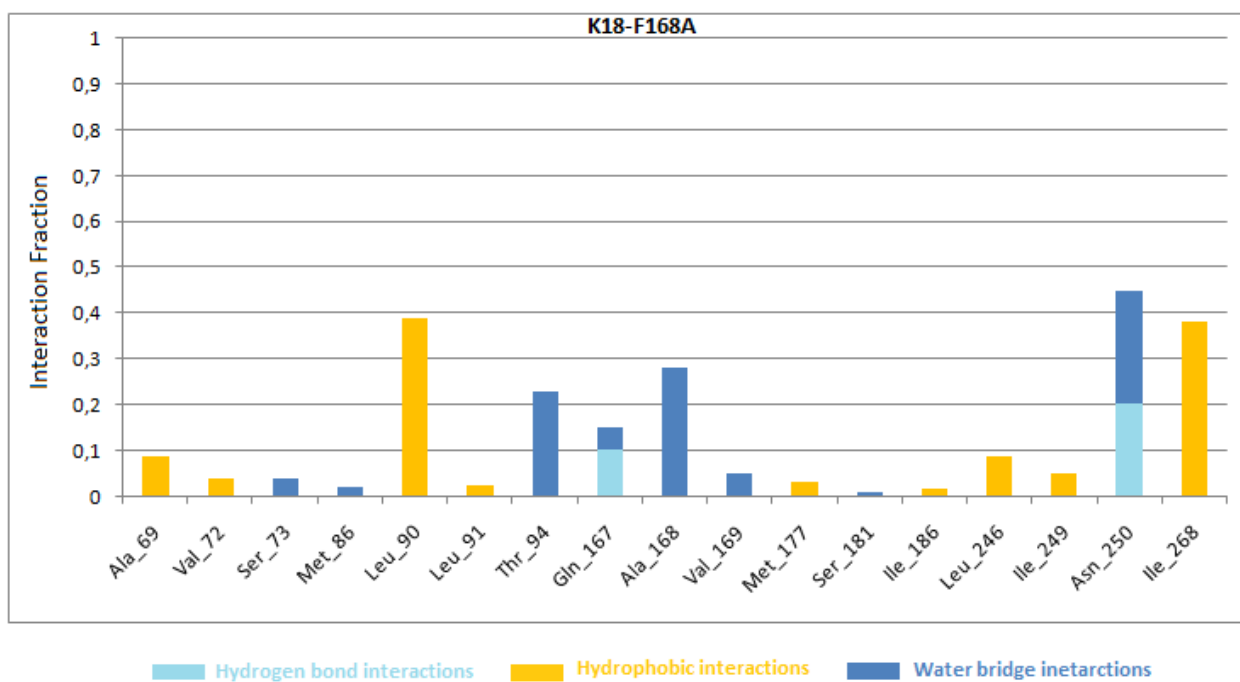


Figure 5. (A) Snapshots of K18-F168^{5,29}A A₃R complex from the unrestrained 100 ns MD simulation. The starting structure of the ligand is shown in green sticks. The binding conformation of the ligand after the 100 ns MD simulation is shown in yellow sticks. The side chains of residues involved in ligand binding, separated by 3.6 Å from the ligand and having interaction frequencies ≥ 0.2 are displayed as gray sticks. Protein structure is displayed in grey ribbons. Hydrogen atoms are omitted except for those involved in hydrogen bond interactions which are highlighted as black dashed lines. (B) Interaction histogram recorded from the 100 ns MD simulation trajectory. Hydrogen bonding interactions bar is depicted in light blue, van der Waals in yellow, water bridges in blue. Bars are plotted for residues with interaction frequencies ≥ 0.2 .

Mutations that maintain antagonistic potency. K18 had a WT-like antagonistic potency for mutant W185^{5.46}A, I253^{6.58}A A₃R which is in agreement with the $\Delta\Delta G_{\text{eff}}$ values of ca +1 and +4.5 kcal mol⁻¹, respectively (Table 2). MD simulations for I253^{6.58}A A₃R-K18 complex showed that, in contrast with WT A₃R complex, the hydrogen bond interactions with N250^{6.55} and the van der Waals interactions with L90^{3.32} and with L246^{6.51} were maintained. K18 translocated towards TM3 and TM7 with an RMSD of 3.6 Å and as a consequence, the interaction frequency with L264^{7.35} was increased while interactions with V169^{5.30} were reduced and with V72^{2.23} were eliminated. Moreover, a strong hydrogen bond interaction with T87^{3.29} appeared as shown in Figure 6.

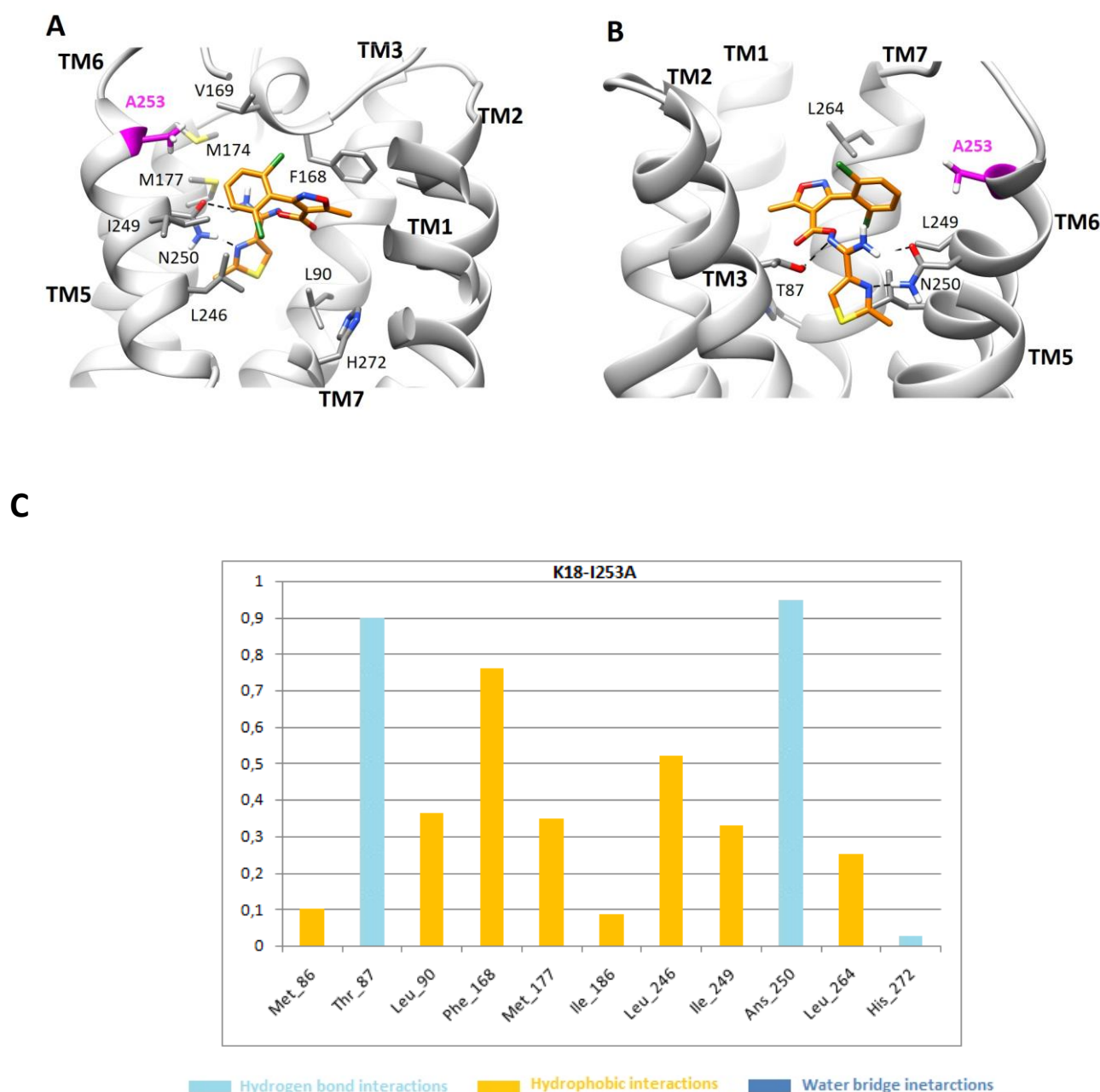
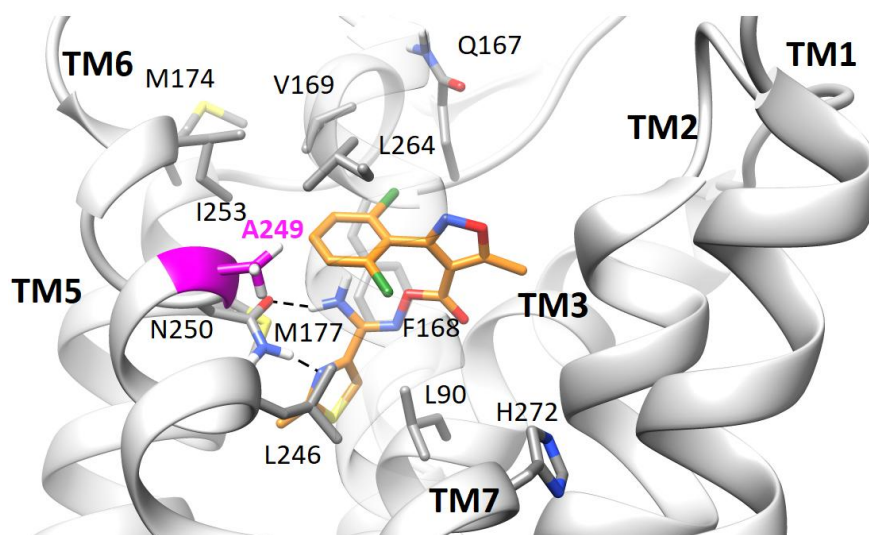


Figure 6. (A), (B) Two different perspectives of the average binding conformation of K18 inside the I253^{6.58}A A₃R binding site from unrestrained 100ns MD simulations (carbon atoms are depicted in yellow color). The side chains of residues involved in ligand binding, separated by 3.6 Å from the ligand and

having interaction frequencies ≥ 0.2 are displayed as gray sticks. Protein structure is displayed in grey ribbons. Hydrogen atoms are omitted except for those involved in hydrogen bond interactions which are highlighted as black dashed lines. (C) Interaction histogram recorded from the 100 ns MD simulation trajectory. Hydrogen bonding interactions bar is depicted in light blue, van der Waals in yellow, water bridges in blue. Bars are plotted for residues with interaction frequencies ≥ 0.2 .

In the case of K18-I249^{6,54}A A₃R the ligand remained close to the starting binding conformation with RMSD_{lig} value of 2.8 Å and the $\Delta\Delta G_{\text{eff}}$ value was ca +10 kcal mol⁻¹. Significant van der Waals interactions with V169^{5,30}, M177^{5,38} were reduced but new interactions appeared, i.e. van der Waals with L264, Y265, I268 and water mediated interactions with the backbone amide groups of F168^{5,29} (Figure 7).

A



B

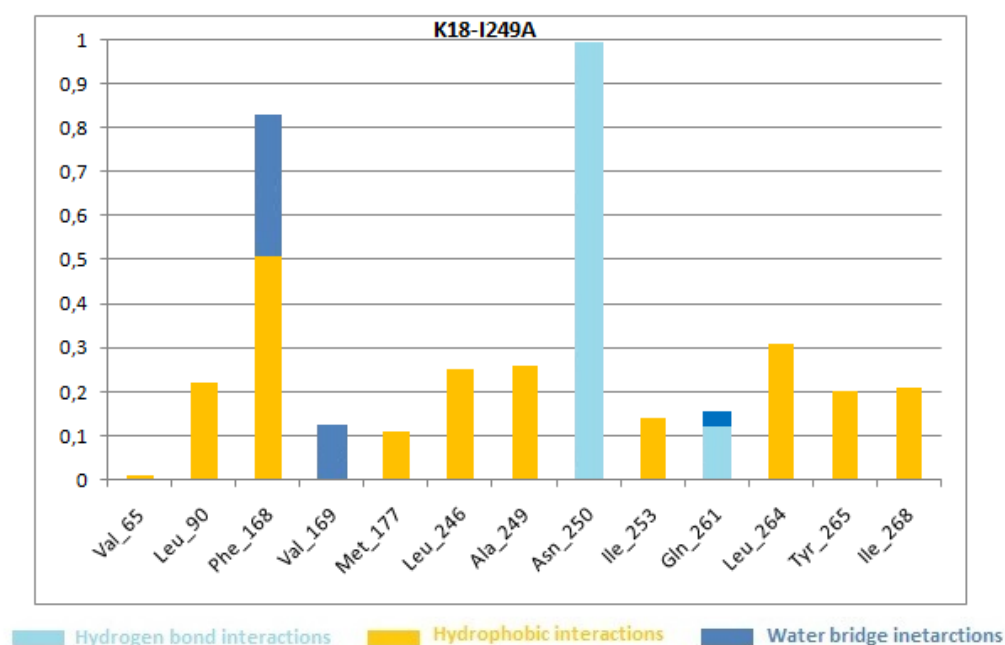
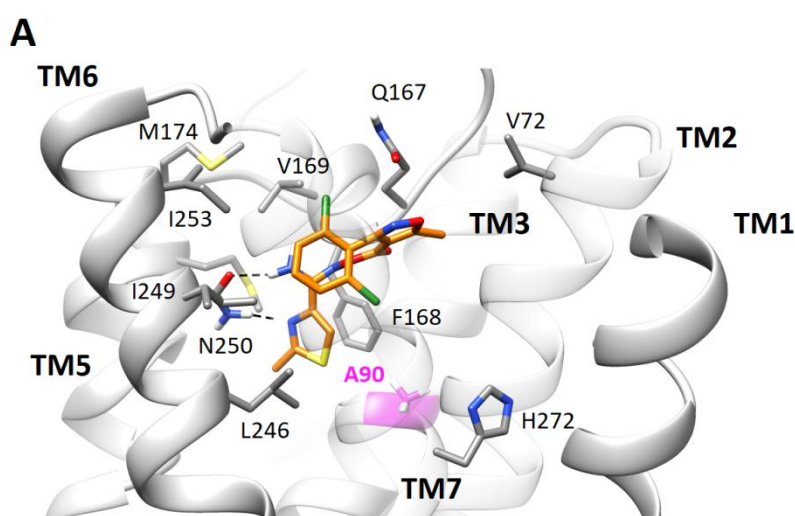


Figure 7. (A) Binding conformation of K18 inside I249^{6.54}A A₃R after the unrestrained 100 ns MD simulation (shown as yellow sticks). The side chains of residues involved in ligand binding, separated by 3.6 Å from the ligand and having interaction frequencies ≥ 0.2 are displayed as gray sticks. Protein structure is displayed in grey ribbons. Hydrogen atoms are omitted except for those involved in hydrogen bond interactions which are highlighted as black dashed lines. (B) Interaction histogram recorded from the 100 ns MD simulation trajectory. Hydrogen bonding interactions bar is depicted in light blue, van der Waals in yellow, water bridges in blue. Bars are plotted for residues with interaction frequencies ≥ 0.2 .

Mutations that increase antagonistic potency. L264^{7.35}A and L90^{3.32}A A₃R mutant showed an increase in antagonistic potency (Table 2).²⁴ When compared to the K18-WT A₃R complex, the interactions in L90^{3.32}A A₃R with N250^{6.55}, F168^{5.29}, L246^{6.51}, M177^{5.38}, I249^{6.54} were maintained. Van der Waals interaction with I249^{6.54} and the interaction with F168^{5.29} showed a particularly increased frequency, the last due to a strong hydrogen bond interaction between the carbonyl group of K18 and the backbone NH groups of F168^{5.29} aided by the reorientation of K18 towards TM6 (Figure 8). This reorientation resulted in an RMSD_{lig} value of 3.7 Å. The increase in potency is reflected by the $\Delta\Delta G_{\text{eff}}$ value of -6 kcal mol⁻¹. In the case of L264^{7.35}A mutant receptor, K18 maintained interactions with L90^{3.32}, F168^{5.29}, M177^{5.38}, L246^{6.51}, N250^{6.55}, I249^{6.54} stabilizing it inside the binding area. The ligand translocated with an RMSD_{lig} value of ca 3.5 Å, the interactions frequency with L90^{3.32}, L246^{6.51} and I268^{7.39} were increased and a new hydrogen bond interaction with T87^{3.29} appeared as shown in Figure 9. The increase of this complex potency is in agreement with the $\Delta\Delta G_{\text{eff}}$ of ca -5 kcal mol⁻¹ (Table 2).



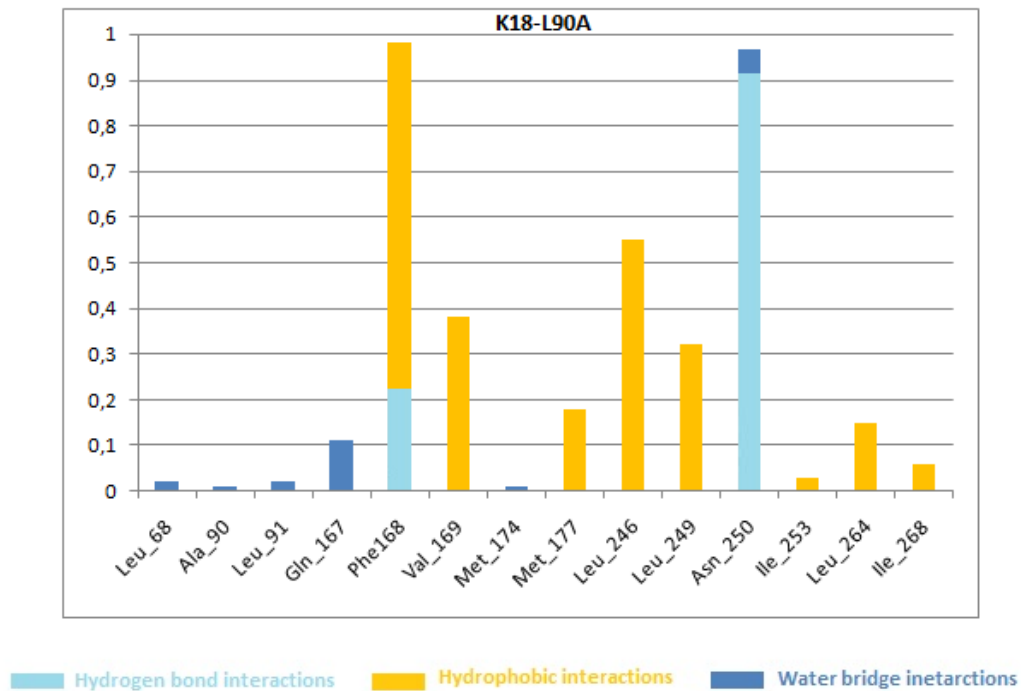
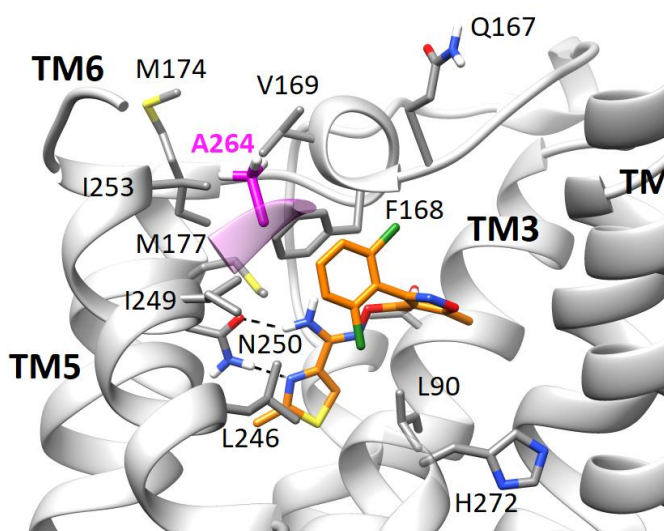
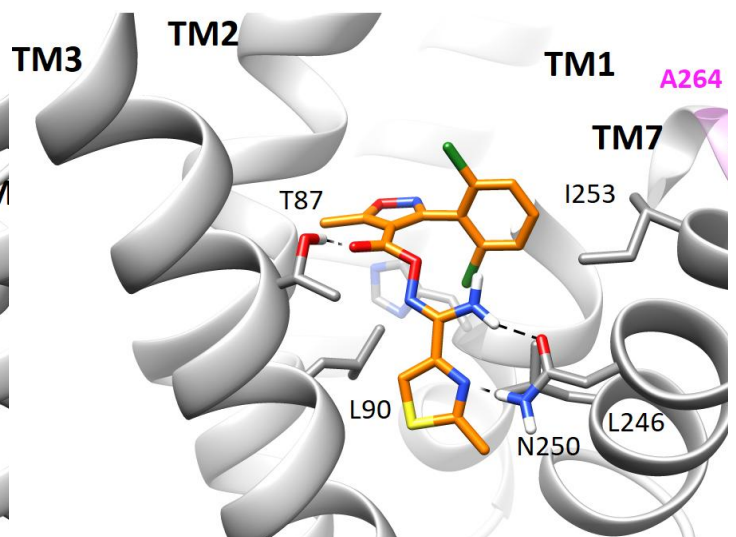
B

Figure 8. Average binding conformation of K18 inside the L90^{3.32}A A₃R binding site from the unrestrained 100 ns MD simulation (carbon atoms are depicted in yellow color). The side chains of residues involved in ligand binding, separated by 3.6 Å from the ligand and having interaction frequencies ≥ 0.2 are displayed as gray sticks. Protein structure is displayed in grey ribbons. Hydrogen atoms are omitted except for those involved in hydrogen bond interactions which are highlighted as black dashed lines. (B) Interaction histogram recorded from the 100 ns MD simulation trajectory. Hydrogen bonding interactions bar is depicted in light blue, van der Waals in yellow, water bridges in blue. Bars are plotted for residues with interaction frequencies ≥ 0.2 .

A**B**

C

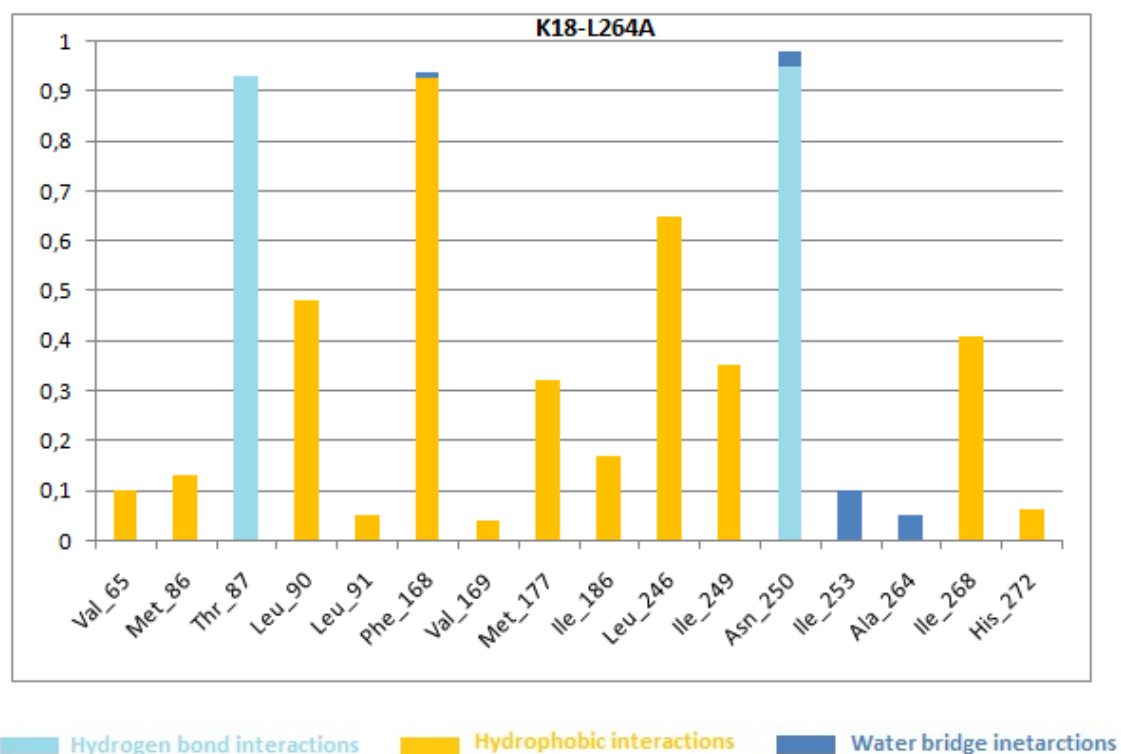
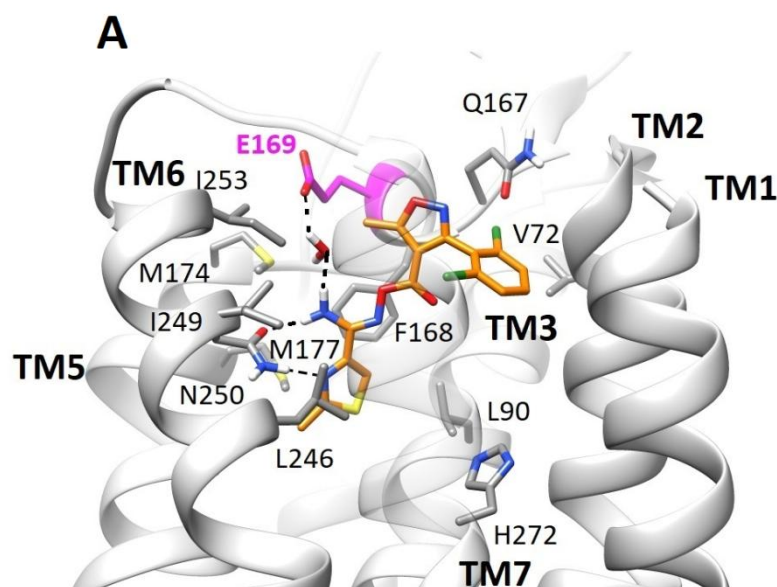


Figure 9. (A), (B) Two different perspectives of the average binding conformation of K18 inside the L264^{7,35}A A₃R binding site from the unrestrained 100 ns MD simulation (carbon atoms are depicted in yellow color). The side chains of residues involved in ligand binding, separated by 3.6 Å from the ligand and having interaction frequencies ≥ 0.2 are displayed as gray sticks. Protein structure is displayed in grey ribbons. Hydrogen atoms are omitted except for those involved in hydrogen bond interactions which are highlighted as black dashed lines. (C) Interaction histogram recorded from the 100 ns MD simulation trajectory. Hydrogen bonding interactions bar is depicted in light blue, van der Waals in yellow, water bridges in blue. Bars are plotted for residues with interaction frequencies ≥ 0.2 .

Mutations to glutamic acid. It has been suggested that residue (5.30) may be linked to the subtype-selectivity of antagonists and its correct modeling can be used in drug design for the identification of new A₃R-selective antagonists. Residue I253^{6,58} also lies in this area but does not interact directly with K18 according to the MD simulation of the agonists-WT A₃R complex (Figure 2B,D). Seeking to verify the significance of these residues, we mutated V169^{5,30} and the remote I253^{6,58} to glutamate.

It was expected that K18 with the "up TM5 TM6" conformation having the dichlorophenyl group oriented close to the EL2 should decrease binding affinity and receptor's signaling (Figure 2D). However, mutant I253^{6.58}E and V169^{5.30}E A₃R_s showed maintenance of potency when bound to antagonist K18.



B

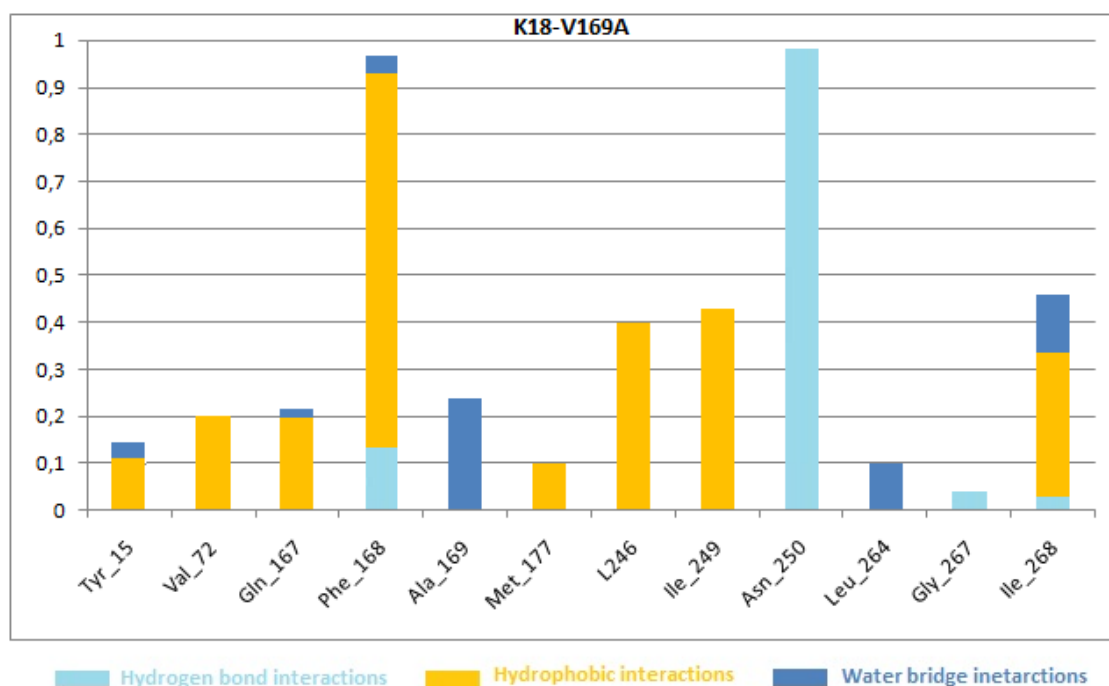
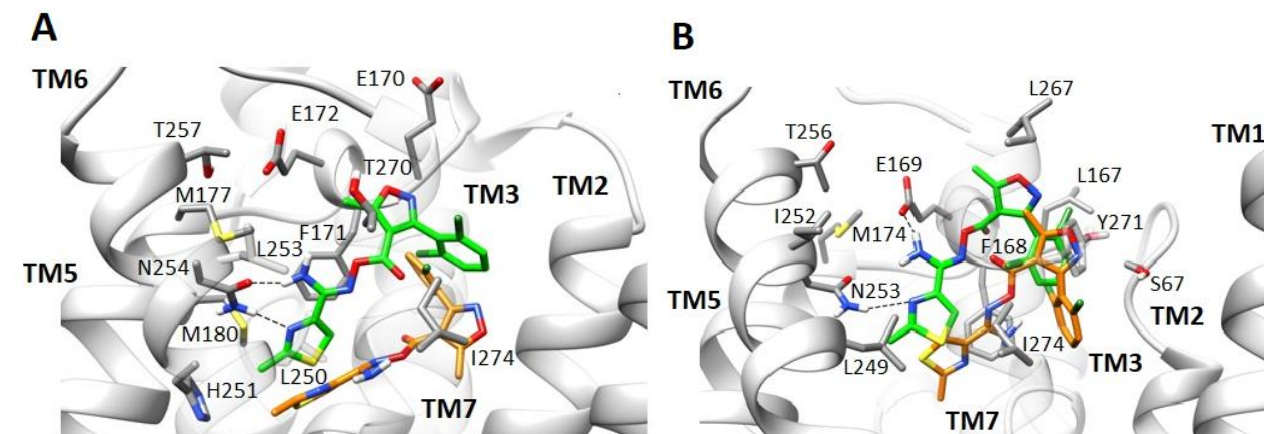


Figure 10. (A) Average binding conformation of K18 inside V169^{5.30}E A₃R binding site from unrestrained 100 ns MD simulation. (B) Receptor-ligand interaction histogram inside V169^{5.30}E A₃R orthosteric binding area, recorded from the 100 ns MD simulation trajectory. Hydrogen bonding interactions bar is depicted in light blue, van der Waals in yellow, water bridges in blue. Bars are plotted for residues with interaction frequencies ≥ 0.2 .

MD simulations showed that binding of K18 can be stable only if the very lipophilic dichlorophenyl group can avoid contacts with glutamate. This is feasible through a 180° rotation of the bond connecting oxazolyl and CO by 180° which results in relocation of the lipophilic dichlorophenyl group away from E^{5.30} and towards the empty space between TM2, TM1 and TM7 giving RMSD_{lig} values of ca 3.5 and 3.6 Å (Figures 10, S7). This orientation for K18 inside the WT A₃R is disfavored by ca 4 kcal mol⁻¹ according to the calculations compared to the orientation with dichlorophenyl group facing TM5, TM6 as mentioned before (Figures 2A-C). Interactions plot showed that the hydrogen bond interaction between the amino group of the K18 and N250^{6.55}, the π-π stacking interaction with phenyl group of F168^{5.29} and the van der Waals with M177^{5.38}, L246^{6.51} were maintained. New frequent hydrophobic interactions with W185^{5.46}, L264^{7.35}, Y265^{7.36} and I268^{7.39} appeared and a new strong hydrogen bond was formed between the amino group of the ligand and the E253^{6.58} carboxylate mediated by a water molecule (Figure 10). For K18 binding inside I253^{6.58}E A₃R trajectory analysis showed binding interactions, some of which include N250^{6.55}, F168^{5.29}, L246^{6.51}, W185^{5.46}, L264^{7.35}, Y265^{7.36} while additional hydrogen bond interactions were formed with Q253^{6.58} and the backbone of F168^{5.29} (Figure S8).

Since in A₁R and A_{2A}R there is a glutamic acid in position (5.30), MD simulations were also performed in order to investigate computationally the reason that K18 did not bind to A₁R and A_{2A}R. The MD simulations showed that K18 failed to bind with the "up TM5, TM6" conformation due to the repulsions with E169^{5.30} but also with "up TM1, TM2" possibly due to the more polar area close to TM1, TM2 in A₁R and A_{2A}R compared to A₃R (Figure 11). Since K18 still binds the V169^{5.30}E, the experimental and MD simulations suggest that other indirect interactions in the A₁R and A_{2A}R are also playing significant role. In A₁R and A_{2A}R the repulsion between dichlorophenyl and glutamate anion groups cannot be relieved in a similar way to A₃R, through a conformational change which moves away glutamate group from K18 due to the plasticity of A₃R in this region.



C

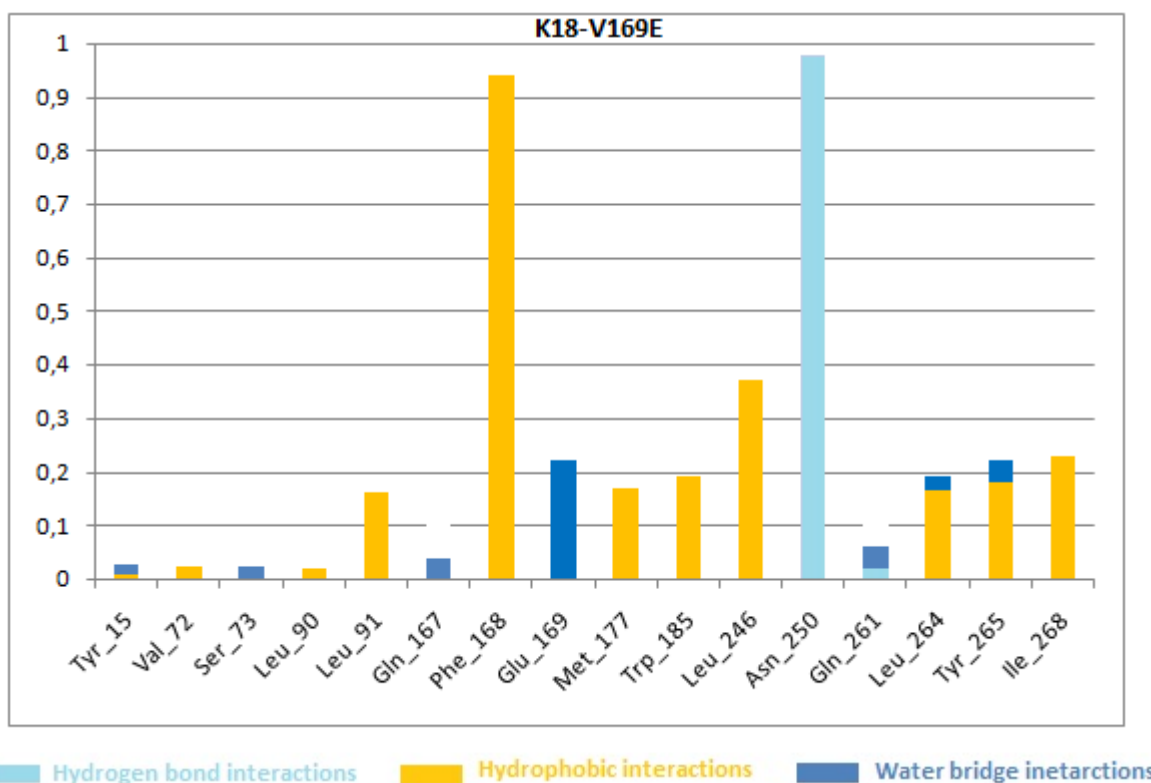


Figure 11. (A), (B) Snapshots of K18 inside the A₁AR and A_{2A}AR binding site respectively from unrestrained 100 ns MD simulations. The starting structure of the ligand is shown in green sticks. The binding conformation of the ligand after the 100 ns MD simulation is shown in yellow sticks. The side chains of residues involved in ligand binding, separated by 3.6 Å from the ligand and having interaction frequencies ≥ 0.2 are displayed as gray sticks. Protein structure is displayed in grey ribbons. Hydrogen atoms are omitted except for those involved in hydrogen bond interactions which are highlighted as black dashed lines. (C) Receptor-ligand interaction histogram interactions plot. Hydrogen bonding interactions bar is depicted in light blue, van der Waals in yellow, water bridges in blue. Bars are plotted for residues with interaction frequencies ≥ 0.2 .

5 Conclusions

The A₃R is currently an important drug target,^{62,63} and the lack of experimental structure limits the structure-based drug design procedures. We investigate the predictions of a computational model which applies: (a) MD simulations with amber99sb using an homology model of A₃R in complex with the most likely conformer of K18 inside the binding area, (b) MM-PBSA and MM-GBSA calculations for complexes of K18 and congener molecules to A₃R, and, (c) complexes of K18 with 14 mutant A₃R. The model was applied to investigate the binding profile of this specific antagonist using previous mutagenic results^{23,24} of several residues of WT A₃R receptor as experimental probes.²⁴

In a previous study,²³ it was found experimentally and confirmed computationally using the same model that IB-MECA activity to A₃R included critical interactions with residues at the TM5, TM6 and EL2, i.e. the direct interactions with F168^{5,29}, L246^{6,51}, V169^{5,30}, N250^{6,55}, and the indirect interactions with M177^{5,38} and L90^{3,32} at the bottom of the orthosteric binding area. M174^{5,35} has also indirect interactions and is important only for NECA activity. Other critical direct interactions for IB-MECA activity included the additional residues at the bottom of the binding area, T94^{3,36}, S271^{7,42}, H272^{7,43} and I268^{7,39}.²³ K18 acts as a competitive antagonist for IB-MECA. According to the computational model is stabilized inside the A₃R orthosteric binding area through an "up TM5, TM6" conformer which interacts with few common residues with the agonist. It forms a π - π interaction with F168^{5,29}, van der Waals interactions with L90^{3,32}, V169^{5,30}, L246^{6,51}, and hydrogen bond interactions with N250^{6,55}. Additionally, K18 interacts directly with M177^{5,38}, I249^{6,54} the first being an important indirectly interacting residus with M177^{5,38}. The computations show that the majority of mutated residues to alanine in direct contact with the antagonist in the WT receptor, should reduce or eliminate potency, i.e. correspondingly V169^{5,30}, F168^{5,29}, M177^{5,38}, L246^{6,51}, N250^{6,55} according to the computational results. This is in agreement with previous experimental results for the mutations V169^{5,30}A, M177^{5,38}A.²³

In agreement with the previous results,^{23,24} the computational model shows that the selectivity of K18 or IB-MECA is not only due to direct interactions with the binding area residues, but also due to indirect effects, through residues positioned at the edges of the binding area, like M174^{5,35} at 4 Å, or more remote residues. The mutation M174^{5,35}A reduces potency and activity correspondingly for K18 and IB-MECA.

The characterization of the area TM6-EL2-TM5 in A₃R which includes lipophilic residues is very important for structure-based drug design of selective ligands. Although this area is occupied by the lipophilic part of selective ligands, like the iodo-benzyl group in IB-MECA residues the experimental results shows and the computational model supports²³ that the mutation V169^{5,30}E causes, instead of reduction, an increase in IB-MECA and NECA activity and that I253^{6,58} is not an important residue of

this region. Also that that I253^{6,58} is not important and that V169^{5,30}E do not reduce but maintains K18 potency. ²⁴ Our computational model shows that compared to the WT A₃R the antagonistic potency of K18 was maintained due to the re-orientation of the dichlorophenyl group of the ligand towards TM1, TM2 and the formation of an additional hydrogen bond interaction E169^{5,30} in agreement with the previous experimental results. The calculations showed that K18 cannot bind to A₁R and A_{2A}R having the E169^{5,30} likely due to the presence of more polar residues in these AR subtypes in this region of binding site and the reduced plasticity of this region compared to A₃R which can contribute to alleviate repulsive interactions through conformational changes.

The previous mutagenesis results are in fair agreement with our computational model. ^{23,24} The experimentally determined pA₂ values and the calculated ΔG_{eff} values for K18 displayed very good correlation, with $r = -0.82$ (Figure 5), while for IB-MECA and NECA the correlation is fair (correspondingly $r = -0.69$ and $r = -0.76$). ²³ Using the MM-GBSA calculated ΔG_{eff} values it is possible to distinguish the three sets of mutant receptors, i.e. those that reduce or negate K18 potency at the A₃R, those that bind stably and maintain potency and those that increase potency compared to WT A₃R. It is also very interesting that the potency is enhanced by the mutations of L90^{3,32}A in the low region or L264^{7,35}A in the middle/upper region which are directly interacting residues with K18. The computational model based on the experimental findings ^{23,24} will be useful for the design of new antagonists which will include substituents above and/or below K18 with adequate orientation towards the low or upper region of the binding area.

6 Supporting Information available

Supplementary material includes the MD simulation protocols, information about MM-PBSA and MM-GBSA method and biological experiments, structures and MD simulations results for K40-K43, Table S1, and Figures S1-S7. This material is available free of charge *via* the Internet at <http://pubs.acs.org>.

7 Acknowledgements

We gratefully acknowledge the support of the Leverhulme Trust (KB and GL) and the BBSRC (GL). This research represents part of the Ph.D work of P.L. We thank Chiesi Hellas which supported this research (SARG No 10354) and the State Scholarships Foundation (IKY) for providing a Ph.D fellowship to P.L. (MIS 5000432, NSRF 2014-2020). The work of E.V. is implemented through IKY scholarships programme and co-financed by the European Union (European Social Fund - ESF) and Greek national funds through the action entitled “Reinforcement of Postdoctoral Researchers”, in the framework of the Operational Program “Human Resources Development Program, Education and Lifelong Learning” of

the National Strategic Reference Framework (NSRF) 2014 – 2020. This work was supported by computational time granted from the Greek Research & Technology Network (GRNET) in the National HPC facility - ARIS - under project IDs pr002021 and pr001004).

8 Author Information

Address for correspondence. Dr Graham Ladds, Department of Pharmacology, University of Cambridge, Tennis Court Road, Cambridge, CB2 1PD Tel; +44 (0) 1223 334020. Email: grl30@cam.ac.uk.

Dr Antonios Kolocouris, Department of Medicinal Chemistry, Faculty of Pharmacy, National and Kapodistrian University of Athens, Panepistimioupolis Zografou, Athens, 15 771. Tel: 210-727-4834, Email: ankol@pharm.uoa.gr.

Author Contributions. AK and GL conceived and designed the research; PL performed most of the simulations and EV, ET, MS performed some simulations; AK analyzed the data produced from the simulations and mutagenesis results from KB; AK wrote the manuscript; KB, GL, ET thoroughly revised and edited the manuscript and EV, MS edited the manuscript.

9 Abbreviations

CNS, central nervous system; 3',5'-cyclic adenosine monophosphate, cAMP; Extracellular loop, EL2; FEP, Free Energy Perturbation; GB, Generalized-Born; PDB, Protein Data Bank; GPCR, G protein coupled receptor; NECA, 5'-(N-ethylcarboxamido)adenosine; IB-MECA, 1-deoxy-1-[6-[(3-iodophenyl)methyl]amino]-9H-purin-9-yl]-N-methyl-β-D-ribofuranuronamide; MD, molecular dynamics; PDB, protein data bank; PME, particle mesh Ewald method; POPE, 1-palmitoyl-2-oleoyl-*sn*- glycerol-3-phosphoethanolamine; RESPA, reversible multiple time scale molecular dynamics; RMSD, root-mean-square deviation; Transmembrane, TM; Molecular Mechanics-Poisson Boltzmann Surface Area, MM-PBSA; Molecular Mechanics-Generalized Born Surface Area, MM-GBSA.

10 References

- (1) Fredholm, B. B.; IJzerman, A. P.; Jacobson, K. A.; Linden, J.; Müller, C. E. *Pharmacol. Rev.* **2011**, pr.
- (2) Romagnoli, R.; Baraldi, P. G.; Moorman, A. R.; Borea, P. A.; Varani, K. *Future Med. Chem.* **2015**, *7*, 1247.
- (3) Lebon, G.; Warne, T.; Edwards, P. C.; Bennett, K.; Langmead, C. J.; Leslie, A. G. W.; Tate, C. G. *Nature* **2011**, *474*, 521.
- (4) Carpenter, B.; Nehmé, R.; Warne, T.; Leslie, A. G. W.; Tate, C. G. *Nature* **2016**.

- (5) García-Nafria, J.; Lee, Y.; Bai, X.; Carpenter, B.; Tate, C. G. *Elife* **2018**.
- (6) Lebon, G.; Edwards, P. C.; Leslie, A. G. W.; Tate, C. G. **2015**.
- (7) Xu, F.; Wu, H.; Katritch, V.; Han, G. W.; Jacobson, K. A.; Gao, Z.-G.; Cherezov, V.; Stevens, R. C. *Science (80-.)*. **2011**, 332, 322.
- (8) Jaakola, V. P.; Griffith, M. T.; Hanson, M. A.; Cherezov, V.; Chien, E. Y. T.; Lane, J. R.; Ijzerman, A. P.; Stevens, R. C. *Science (80-.)*. **2008**, 322, 1211.
- (9) Liu, W.; Chun, E.; Thompson, A. A.; Chubukov, P.; Xu, F.; Katritch, V.; Han, G. W.; Roth, C. B.; Heitman, L. H.; IJzerman, A. P.; Cherezov, V.; Stevens, R. C. *Science* **2012**, 337, 232.
- (10) Doré, A. S.; Robertson, N.; Errey, J. C.; Ng, I.; Hollenstein, K.; Tehan, B.; Hurrell, E.; Bennett, K.; Congreve, M.; Magnani, F.; Tate, C. G.; Weir, M.; Marshall, F. H. *Structure* **2011**, 19, 1283.
- (11) Jaakola, V.-P.; Griffith, M. T.; Hanson, M. A.; Cherezov, V.; Chien, E. Y. T.; Lane, J. R.; IJzerman, A. P.; Stevens, R. C. *Science (80-.)*. **2008**, 322, 1211.
- (12) Sun, B.; Bachhawat, P.; Chu, M. L.-H.; Wood, M.; Ceska, T.; Sands, Z. A.; Mercier, J.; Lebon, F.; Kobilka, T. S.; Kobilka, B. K. *Proc. Natl. Acad. Sci.* **2017**, 114, 2066.
- (13) Liu, W.; Chun, E.; Thompson, A. A.; Chubukov, P.; Xu, F.; Katritch, V.; Han, G. W.; Roth, C. B.; Heitman, L. H.; IJzerman, A. P.; Cherezov, V.; Stevens, R. C. *Science (80-.)*. **2012**, 337, 232.
- (14) Doré, A. S.; Robertson, N.; Errey, J. C.; Ng, I.; Hollenstein, K.; Tehan, B.; Hurrell, E.; Bennett, K.; Congreve, M.; Magnani, F.; Tate, C. G.; Weir, M.; Marshall, F. H. *Structure* **2011**, 19, 1283.
- (15) Glukhova, A.; Thal, D. M.; Nguyen, A. T.; Vecchio, E. A.; Jörg, M.; Scammells, P. J.; May, L. T.; Sexton, P. M.; Christopoulos, A. *Cell* **2017**, 168, 867.
- (16) Cheng, R. K. Y.; Segala, E.; Robertson, N.; Deflorian, F.; Doré, A. S.; Errey, J. C.; Fiez-Vandal, C.; Marshall, F. H.; Cooke, R. M. *Structure* **2017**, 25, 1275.
- (17) Glukhova, A.; Thal, D. M.; Nguyen, A. T.; Vecchio, E. A.; Jörg, M.; Scammells, P. J.; May, L. T.; Sexton, P. M.; Christopoulos, A. *Cell* **2017**, 168, 867.
- (18) Cheng, R. K. Y.; Segala, E.; Robertson, N.; Deflorian, F.; Doré, A. S.; Errey, J. C.; Fiez-Vandal, C.; Marshall, F. H.; Cooke, R. M. *Structure* **2017**, 25, 1275.
- (19) Draper-Joyce, C. J.; Khoshouei, M.; Thal, D. M.; Liang, Y. L.; Nguyen, A. T. N.; Furness, S. G. B.; Venugopal, H.; Baltos, J. A.; Plitzko, J. M.; Danev, R.; Baumeister, W.; May, L. T.; Wootten, D.; Sexton, P. M.; Glukhova, A.; Christopoulos, A. *Nature* **2018**, 558, 559.
- (20) Katritch, V.; Jaakola, V. P.; Lane, J. R.; Lin, J.; Ijzerman, A. P.; Yeager, M.; Kufareva, I.; Stevens, R. C.; Abagyan, R. *J. Med. Chem.* **2010**, 53, 1799.
- (21) Carlsson, J.; Yoo, L.; Gao, Z. G.; Irwin, J. J.; Shoichet, B. K.; Jacobson, K. A. *J. Med. Chem.* **2010**, 53, 3748.
- (22) Li, J.; Jonsson, A. L.; Beuming, T.; Shelley, J. C.; Voth, G. A. *J. Am. Chem. Soc.* **2013**.
- (23) Stamatis, D.; Lagarias, P.; Barkan, K.; Vrontaki, E.; Ladds, G.; Kolocouris, A. *Submitted* **2018**.
- (24) Barkan, K.; Lagarias, P.; Stamatis, D.; Vrontaki, E.; Klotz, K.-L.; Kolocouris, A.; Ladds, G. <https://doi.org/10.1101/693796> **2019**.
- (25) Lagarias, P.; Vrontaki, E.; Lambrinidis, G.; Stamatis, D.; Convertino, M.; Ortore, G.; Mavromoustakos, T.; Klotz, K.-N.; Kolocouris, A. *J. Chem. Inf. Model.* **2018**, 58, 794.
- (26) Homeyer, N.; Gohlke, H. *Mol. Inform.* **2012**.
- (27) Homeyer, N.; Stoll, F.; Hillisch, A.; Gohlke, H. *J. Chem. Theory Comput.* **2014**, 10, 3331.
- (28) Floris, M.; Sabbadin, D.; Medda, R.; Bulfone, A.; Moro, S. *Eur. J. Med. Chem.* **2012**, 58, 248.
- (29) Ballesteros, J. A.; Weinstein, H. *Receptor Molecular Biology*; 1995; Vol. 25.
- (30) Katritch, V.; Kufareva, I.; Abagyan, R. *Neuropharmacology* **2011**, 60, 108.
- (31) Katritch, V.; Kufareva, I.; Abagyan, R. *Neuropharmacology* **2011**, 60, 108.
- (32) *Protein Prep. Wizard 2015-2; Epik version 2.4, Schrödinger, LLC, New York, NY, 2015; Impact version 5.9, Schrödinger, LLC, New York, NY, 2015; Prime version 3.2, Schrödinger, LLC, New York, NY, 2015.*
- (33) Kaminski, G. A.; Friesner, R. A.; Tirado-Rives, J.; Jorgensen, W. L. *J. Phys. Chem. B* **2001**, 105, 6474.
- (34) Maestro, version 10.5; Schrodinger, Inc.: New York, NY, 2015.
- (35) Jones, G.; Willett, P.; Glen, R. C.; Leach, A. R.; Taylor, R. *J. Mol. Biol.* **1997**, 267, 727.
- (36) *GOLD Suite, version 5.2; Cambridge Crystallogr. Data Cent. Cambridge, U.K., 2015.*
- (37) Verdonk, M. L.; Chessari, G.; Cole, J. C.; Hartshorn, M. J.; Murray, C. W.; Nissink, J. W. M.;

- Taylor, R. D.; Taylor, R. *J. Med. Chem.* **2005**, *48*, 6504.
- (38) Hawkins, P. C. D.; Skillman, A. G.; Nicholls, A. *J. Med. Chem.* **2007**, *50*, 74.
- (39) Glide, Schrödinger, LLC, New York, NY, 2012. Glide, version 5.7. *Glide Schrödinger LLC NY*, 2011.
- (40) *Desmond Mol. Dyn. Syst. version 3.0; D.E. Shaw Res. New York, 2011; Maest. Interoperability Tools, 3.1; Schrodinger Res. New York, 2012.*
- (41) Bowers, K. J.; Sacerdoti, F. D.; Salmon, J. K.; Shan, Y.; Shaw, D. E.; Chow, E.; Xu, H.; Dror, R. O.; Eastwood, M. P.; Gregersen, B. A.; Klepeis, J. L.; Kolossvary, I.; Moraes, M. A. In *Proceedings of the 2006 ACM/IEEE conference on Supercomputing - SC '06*; ACM Press: New York, New York, USA, 2006; p. 84.
- (42) Jorgensen, W. L.; Chandrasekhar, J.; Madura, J. D.; Impey, R. W.; Klein, M. L. *J. Chem. Phys.* **1983**, *79*, 926.
- (43) Wang, J.; Cieplak, P.; Kollman, P. A. *J. Comput. Chem.* **2000**, *21*, 1049.
- (44) Hornak, V.; Abel, R.; Okur, A.; Strockbine, B.; Roitberg, A.; Simmerling, C. *Proteins Struct. Funct. Bioinforma.* **2006**, *65*, 712.
- (45) Wang, J.; Wolf, R. M.; Caldwell, J. W.; Kollman, P. A.; Case, D. A. *J. Comput. Chem.* **2004**, *25*, 1157.
- (46) Case, D. A.; Babin, V.; Berryman, J. T.; Betz, R. M.; Cai, Q.; Ceruti, D. S.; Cheatham, I. I. I. T. E.; Darden, T. A.; Duke, R. E.; Gohlke, H.; Goetz, A. W.; Gusarov, S.; Homeyer, N.; Janowski, P.; Kaus, J.; Kolossvary, I.; Kovalenko, A.; Lee, T. S.; LeGrand, S.; Luchko, T.; Luo, R.; Madej, B.; Merz, K. M.; Paesani, F.; Roe, D. R.; Roitberg, A.; Sagui, C.; Salomon-Ferrer, R.; Seabra, G.; Simmerling, C. L.; Smith, W.; Swails, J.; Walker, R. C.; Wang, J.; Wolf, R. M.; Wu, X.; Kollman, P. A. .
- (47) Koynova, R.; Caffrey, M. Phases and phase transitions of the phosphatidylcholines. *Biochimica et Biophysica Acta - Reviews on Biomembranes*, 1998, *1376*, 91–145.
- (48) D.A. Case J.T. Berryman, R.M. Betz, Q. Cai, D.S. Cerutti, T.E. Cheatham, III, T.A. Darden, R.E. Duke, H. Gohlke, A.W. Goetz, S. Gusarov, N. Homeyer, P. Janowski, J. Kaus, I. Kolossvary, A. Kovalenko, T.S. Lee, S. LeGrand, T. Luchko, R. Luo, B. Madej, K.M, V. B. The Amber Molecular Dynamics Package. *AMBER*, 2014, *14*.
- (49) Maier, J. A.; Martinez, C.; Kasavajhala, K.; Wickstrom, L.; Hauser, K. E.; Simmerling, C. *J. Chem. Theory Comput.* **2015**, *11*, 3696.
- (50) Dickson, C. J.; Madej, B. D.; Skjevik, Å. A.; Betz, R. M.; Teigen, K.; Gould, I. R.; Walker, R. C. *J. Chem. Theory Comput.* **2014**, *10*, 865.
- (51) Jorgensen, W. L.; Chandrasekhar, J.; Madura, J. D.; Impey, R. W.; Klein, M. L. *J. Chem. Phys.* **1983**, *79*, 926.
- (52) Bayly, C. I.; Cieplak, P.; Cornell, W. D.; Kollman, P. A. *J. Phys. Chem.* **1993**.
- (53) Frisch, M. J. et al. *Revis. B.04* **2003**.
- (54) Pettersen, E. F.; Goddard, T. D.; Huang, C. C.; Couch, G. S.; Greenblatt, D. M.; Meng, E. C.; Ferrin, T. E. *J. Comput. Chem.* **2004**, *25*, 1605.
- (55) Humphrey, W.; Dalke, A.; Schulten, K. *J. Mol. Graph.* **1996**, *14*, 33.
- (56) Gohlke, H.; Case, D. A. *J. Comput. Chem.* **2004**, *25*, 238.
- (57) Massova, I.; Kollman, P. A. *Perspect. drug Discov. Des.* **2000**, *18*, 113.
- (58) Miller, B. R.; McGee, T. D.; Swails, J. M.; Homeyer, N.; Gohlke, H.; Roitberg, A. E. *J. Chem. Theory Comput.* **2012**.
- (59) Jaakola, V.-P.; Griffith, M. T.; Hanson, M. A.; Cherezov, V.; Chien, E. Y. T.; Lane, J. R.; Ijzerman, A. P.; Stevens, R. C. *Science* **2008**, *322*, 1211.
- (60) Lagarias, P.; Vrontaki, E.; Lambrinidis, G.; Stamatis, D.; Convertino, M.; Ortore, G.; Mavromoustakos, T.; Klotz, K.-N.; Kolocouris, A. *J. Chem. Inf. Model.* **2018**, *58*.
- (61) Keränen, H.; Åqvist, J.; Gutiérrez-De-Terán, H. *Chem. Commun.* **2015**.
- (62) Liang, B. T.; Jacobson, K. A. *Proc. Natl. Acad. Sci.* **2002**, *95*, 6995.
- (63) Okamura, T.; Kurogi, Y.; Hashimoto, K.; Sato, S.; Nishikawa, H.; Kiryu, K.; Nagao, Y. *Bioorganic Med. Chem. Lett.* **2004**, *14*, 3775.

TOC GRAPHIC

Ala scanning effect in activity

INCREASE

NORMAL

DECREASE

